University of Nairobi

School of Engineering

Developing a Cloud Removal Tool by Combining Optical and Microwave ALOS Data

BY

Maithya Mutyauvyu

F56/83390/2015

A Project submitted in partial fulfillment for the Degree of Master of Science in Geographical Information Systems (GIS), in the Department of Geospatial and Space Technology of the University of Nairobi

June, 2017

Declaration

I, Maithya Mutyauvyu hereby declare that this project is my original work. To the best of my knowledge, the work presented here has not been presented for a degree in any other Institution of Higher Learning.

Maithya Mutyauvyu Date ……

This project report has been submitted with approval of university supervisor.

Dr. Faith Njoki Karanja Date ……

Dedication

I dedicate this project to my late father for the fingerprints of grace he left in my life.

Acknowledgement

I would like to express my sincere gratitude to my Supervisor Dr. Faith Karanja for her continuous support during my master's project and related research, her patience, motivation, and immense knowledge. I could not have imagined having a better advisor and mentor for my masters' study. Dr. Richard Onwonga for his managerial support and ensuring that the scholarship funds are available in time, the National Environment Management Authority (NEMA) for giving me ample time and study leave during the period of my study. Finally, I would like to extend my gratitude to Clinton Foundation for offering me the scholarship opportunity at the University of Nairobi.

Abstract

In optical remote sensing, clouds have always been a major problem because they obstruct the details underneath them owing to the simple reason that the visible band of electromagnetic spectrum cannot penetrate clouds. This study presents a novel approach to address the problem of clouds and their shadows in optical images by combining optical and microwave data of Advanced Land Observation Satellite (ALOS) by taking advantage of the ability of microwaves to penetrate clouds, fog, haze and mist. The study focuses on development of an algorithm that is able to detect clouds, cloud shadow, mask both cloud and cloud shadow contaminated pixels and by use of interpolation technique between the optical and the microwave image, re-establish pixel values for the masked pixels. The detection of thick clouds is done by computing Total Reflectance Radiance Index (TRRI) using the four Bands of ALOS optical image (AVNIR-2 Image) and defining thresholds that accurately define thick clouds. Thin Clouds are detected using Cloud Soil Index (CSI) and also defining thresholds that define the thin clouds. Cloud shadows are detected by projecting the detected clouds by the average distance and bearing measured from a sample of clouds to their corresponding cloud shadows. In all cloud and cloud shadow contaminated pixels, their corresponding pixels are identified in the microwave image and using nearest search, other pixels with similar or nearest pixel values are searched for and once identified, their corresponding pixels in the optical image are identified and their pixel values are used to fill the masked pixels.

The results show that the developed algorithm for detection of thick clouds using the defined TRRI thresholds worked very well and all the thick clouds were detected and masked out while the developed algorithm for detecting thin clouds using defined thresholds of CSI worked very well too with most of the thin clouds being detected and masked out. However, there were some remnants of thin cloud patches which still went on undetected and further research needs to be done for more precise methods of detecting thin clouds. The developed program function for detection and masking of cloud shadow worked very well with all the cloud shadow pixels being detected and masked out. The developed program for interpolation to fill the missing pixel values in the already masked cloud and cloud shadow pixels worked well with the missing information being revealed. Therefore, the algorithm for cloud and cloud shadow removal was successfully developed with all the subcomponents working well. However further research needs to be done for improved methods of thin cloud detection and future satellite developments needs to consider incorporation of both optical and microwave sensor in the same platform.

Table of Contents

Declaration ii

Dedication iii

Acknowledgement iv

Abstract v

Chapter 1: Introduction 2

1.1 Background to the Study 2

1.2 Problem Statement 4

1.3 Objectives of the Study 4

1.4 Justification for the Study 5

1.5 Scope of work 5

1.6 Organization of the Report 5

Chapter 2: Literature Review 7

2.1 Remote Sensing for Natural Resource Management 7

2.2 Types of Earth Observation Remote Sensing Sensors 8

2.2.1 Optical Sensors 8

2.2.2 Microwave Sensors 9

2.3 Challenges of Clouds using Optical Remote Sensing Satellites 9

2.4 Status of Remote Sensing Technology in Africa 10

2.5 ALOS Data 11

2.6 Techniques used to address Clouds in Remote Sensing Data 14

2.6.1 Multitemporal-based Approaches 14

2.6.2 Multispectral-based Approaches 19

2.6.3 Contamination detection approach 19

2.6.4 Inpainting-based Approaches 27

Chapter 3: Methodology 28

3.1 Study Area 28

3.2 Data Acquisition 32

3.3 Data Pre-processing 33

3.3.1 Geo-Rectification 33

3.3.2 Radiance and Reflectance Conversion 33

3.4 Cloud and Cloud Shadow Definition 34

3.4.1 Thick Cloud 35

3.4.2 Thin Cloud 36

3.4.3 Cloud Shadow 37

3.5 Developing Algorithm for Cloud Removal 38

3.6 Testing the Algorithm 39

3.7 Application of the Cloud and Shadow Free Image for Land Cover Analysis 39

Chapter 4: Results and Discussions 40

4.1 Identified Clouds and Cloud Shadows 40

4.1.1 Thick Clouds Masked. 40

4.1.2 Thin Clouds Masked. 41

4.1.3 Cloud Shadows Masked 42

4.1.4 Cloud and Cloud Shadow Masking combined 43

4.2 Cloud and Cloud Shadow Free Image 44

4.3 Cloud and Cloud Shadow Free Image Land Cover Analysis 46

4.3.1 Verification of Results 46

4.3.2 Test of Interpolated Image for Other Applications 49

4.3.3 Comparative Analysis for Land cover 49

4.4 Discussions of the Results 51

Chapter 5: Conclusions and Recommendations 52

5.1 Conclusions..... 52

5.2 Recommendations..... 53

References..... 54

Appendix A..... 59

Appendix A1: The developed MATLAB Algorithm..... 59

List of Figures

Figure 1.1 Electromagnetic Spectrum 3
Figure 1.2 Cloud Capture in Optical Images 4
Figure 3.1 Flow Chart of Methodology 29
Figure 3.2 Study Area Map 30
Figure 3.3: Study Area Linked with Image 31
Figure 3.4 Interpolation Technique for Cloud Removal 39

List of Tables

Table 2.1 General Concepts of ALOS Sensor 12
Table 2.2 Major Characteristics of ALOS 13
Table 2.3 Characteristics of ALOS AVNIR-2 13
Table 3.1 Band Gain and Offset for AVNIR-2 Image 34
Table 3.2 Reflectance Computation Parameters 34
Table 3.3 AVNIR-2 Image Bands Wavelengths 35
Table 3.4 Average Distance and Bearing to Cloud Shadows 38

List of Plates

Plate 3.1 AVNIR-2 Image 32
Plate 3.2 ALOS PALSAR Image 32
Plate 3.3: TRRI Index Image 36
Plate 3.4: CSI Index Image 37
Plate 4.1: AVNIR-2 Image Thick Clouds Masked 40
Plate 4.2: AVNIR-2 Image with Thin Clouds Masked 41
Plate 4.3: Cloud Shadow Mask 42
Plate 4.4: Cloud and Cloud Shadow Masked 43
Plate 4.5: Cloud and Cloud Shadow Masked Image Linked with Study Area 44
Plate 4.6: Interpolated Cloud and Cloud Shadow Free Image 45
Plate 4.7: Interpolated Cloud Free Image Linked with Study Area 46
Plate 4.8: Interpolated Cloud Free Image 48
Plate 4.9: High Resolution Image 48
Plate 4.10: Test of Interpolated Image for Digitization 49
Plate 4.11: Cloud and Cloud Shadow Removal on Farmland Landcover 50
Plate 4.12:Cloud and Cloud Shadow Removal on Forest Landcover 50

Chapter 1: Introduction

1.1 Background to the Study

One of the greatest challenges in economic planning, environmental studies and natural resource management is obtaining current and accurate information about the surface of the earth. Due to the expansive nature of the surface of the earth, remote sensing techniques are the most economical techniques of obtaining such information and satellite remote sensing as well as aerial photography are the commonly used techniques. Aerial photography is used for small areas (Large scale mapping) and has the advantage of high level details but the cost is high while satellite remote sensing is used for large areas (Small scale mapping) with relatively low-level details but the cost is comparatively low (Goodwin and Hudson 2002). Remote sensing is defined as the science (and to some extent, art) of acquiring information about the Earth's surface without actually being in contact with it and processing, analyzing, and applying that information (Canada Centre for Remote Sensing 2016). The development of remote sensing dates back in 1859 when Gaspard Tournachon took an oblique photograph of a small village near Paris from a balloon and with this picture, the era of earth observation and remote sensing just started (James and Randolph 2011).

His example was soon followed by other people all over the world and this was the genesis of remote sensing with balloons and aircrafts being used in the first development stages and later satellites were developed and currently satellites account for the greatest percentage of remote sensing data (Aggarwal 2005). In either of these imaging platforms, there are sensors which detect and record the reflected energy from the surface of the earth and they are classified into optical, microwave, infrared and thermal sensors among others depending on the part of the electromagnetic spectrum which they detect and record the reflected energy. Optical sensors detect and record the visible and infrared (near infrared, intermediate infrared and thermal infrared) bands of the electromagnetic spectrum while microwave sensors detect and record microwaves (P, L, S, C, X, K_u, K and K_a) bands which have longer wavelengths than visible light and infrared rays, and observation is not affected by day, night or weather. Scientists found that many types of waves can be arranged together like notes on a piano keyboard to form a scale called electromagnetic spectrum which is defined as the distribution of electromagnetic radiation according to energy, wavelength or frequency (Klaus, Norman and Gerrit 2009) as shown in *Figure 1.1*

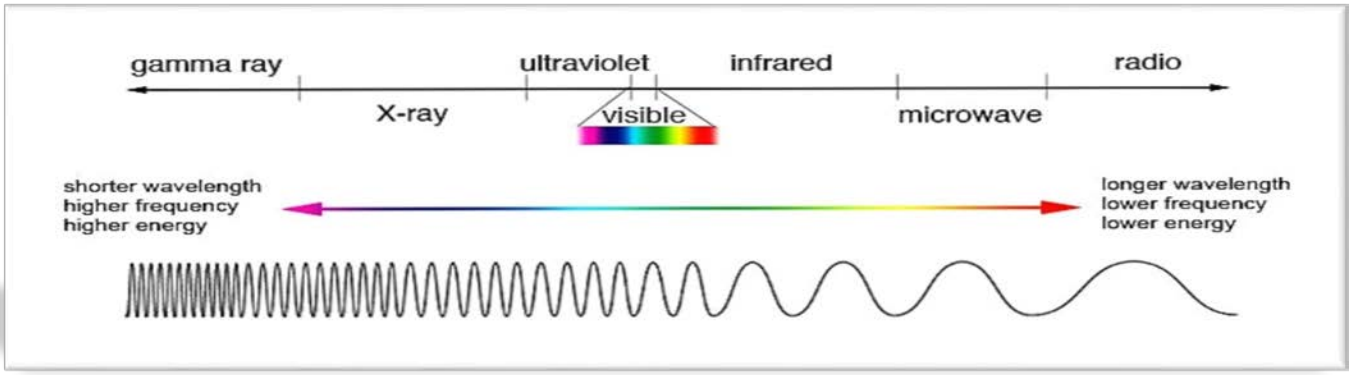

Figure 1.1 Electromagnetic Spectrum *(Source: Principles of Remote Sensing, Aggarwal, 2005)*

Most electromagnetic waves are affected by atmospheric scattering which is defined as the process by which small particles suspended in the atmosphere (water, dust and gas particles) diffuse incident radiation in to different directions (Aggarwal 2005). Atmospheric scattering is a function of several factors and among them is wavelength of the incident radiation and the longer the wavelength, the less the scattering and therefore longer wavelengths are able to penetrate the atmosphere than short wavelengths. Since microwaves have longer wavelengths, they are able to penetrate clouds (water particles) and other particles suspended in the atmosphere whereas visible band of the electromagnetic spectrum is affected by atmospheric scattering (short wavelength) and it is for this reason that microwave data is being used for cloud removal in this research. There are three types of atmospheric scattering; Rayleigh, Mie and Nonselective scattering.

Rayleigh scattering occurs when the scattering particles are very small compared to the wavelength of the incident radiation, Mie scattering occurs when the scattering particles are just about the same diameter with the wavelength of the incident radiation. Lastly, Nonselective scattering occurs when the scattering particles are larger than the wavelength of the incident radiation and this is the type of scattering that is responsible for clouds in optical remote sensing. It draws its name from the fact that incident radiations are scattered equally (non-selectively) and water droplets (which form clouds) as well as dust particles are responsible for this type of scattering. This type of scattering causes fog and clouds to appear white to our eyes because blue, green, and red light are all scattered in approximately equal quantities (blue + green + red light = white light) (Canada Centre for Remote Sensing 2016) as shown in *Figure 1.2*. Clouds not only obstruct image details but also cast their shadows on the ground obscuring image details in the areas of their occurrence and this limits the usage of optical images to various remote sensing applications.

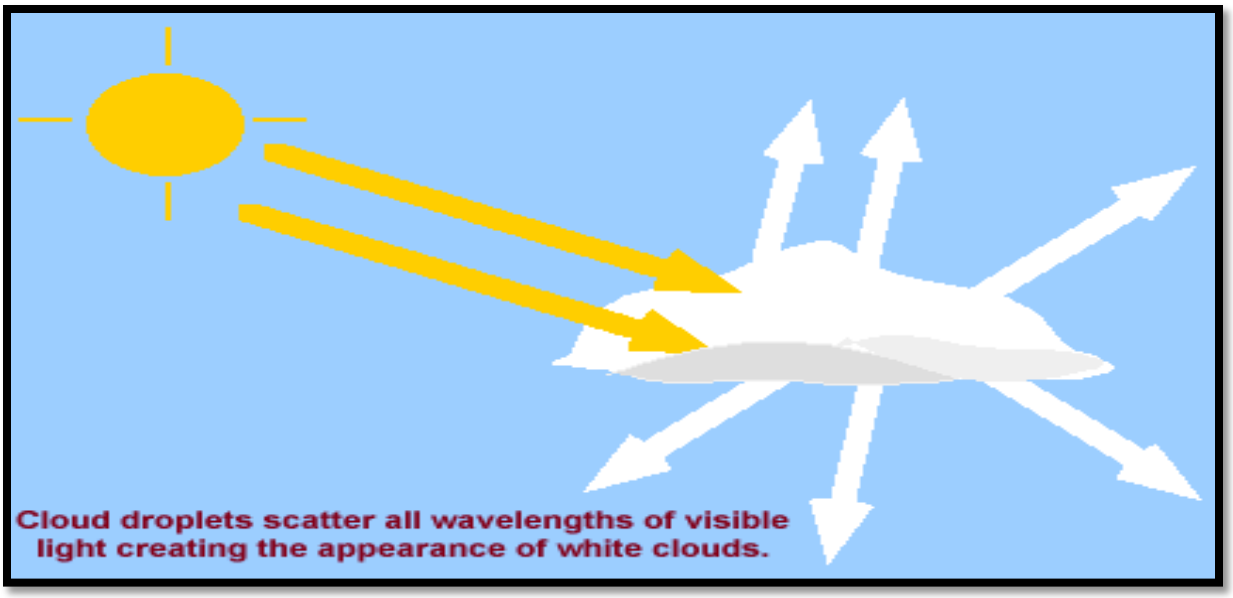

Figure 1.2 Cloud Capture in Optical Images *(Source: Centre for Remote Sensing, 2016)*

1.2 Problem Statement

Remote Sensing is a very common and useful method for land cover mapping, land use mapping, resource mapping, weather forecasting, research among others. The data from optical remote sensing satellites such as SPOT, IKONOS, QuickBird and Geo-eye is often used in conventional methods because of their advantages including resolution, both radiometric and spatial. However, the disadvantage of the optical data is cloud effect. In areas frequently covered by clouds, such as Tropical environments, it becomes a considerable problem to obtain cloud free satellite images for mapping and other remote sensing applications. In contrast, microwave remote sensing data is not affected by cloud but only affected by the relief. In this study, it is expected that the information from radar image will be used to add to the absent information under cloud on the optical image because the microwaves have the ability to penetrate clouds and this will be achieved by use of interpolation technique.

1.3 Objectives of the Study

The general objective of the study was to develop a cloud and cloud shadow removal algorithm that removes clouds and their corresponding shadows from optical images using microwave data through interpolation technique. The following were the specific objectives of the study;

i. Create a program function that can identify/define cloud in Satellite Images.
ii. Design a program function that can identify/define cloud shadow in Satellite Images.

iii. Develop a program function that can remove cloud in Satellite Images using interpolation Technique.
iv. Test the cloud and cloud shadow free image through land cover analysis.

1.4 Justification for the Study

Successful completion of this study will be a great milestone in the country for the problem of clouds in optical images will have been resolved and this will go a long way in ensuring accurate data and information is available for policy makers, researchers and other consumers of remote sensing data and information. Climate change has become a global phenomenon and accurate data to monitor the trend and impacts of climate change is required and remote sensing is one of the technologies that provides such information and presence of clouds in satellite images interferes with the accuracy of generated data and information. The resulting inaccuracies can lead to decision makers to make wrong decisions such as ongoing negotiations for climate change mitigation funds. Another example is in mapping of carbon sinks (mostly forests) where very accurate data on the coverage (area) is required for compensation in the carbon trade market and carbon credit concepts.

1.5 Scope of work

This study is intended for development of a tool for cloud removal from optical satellite images using radar images and is limited to the following;

i. Development of a program function that defines clouds (Both thick and thin clouds)
ii. Development of a program function defines cloud shadow.
iii. Development of a program function that removes cloud and cloud shadows through interpolation technique.

1.6 Organization of the Report

This project report is organized in five chapters and as discussed below.

i. Chapter 1: This chapter discusses the motivations behind the choice of the study topic, problem statement, objectives of the study as well as justification for the study.
ii. Chapter 2: This chapter discusses how remote sensing has been applied in natural resources management, types of earth observation remote sensing sensors and status of remote sensing technology in Africa. It also discusses the general concepts of ALOS data as well

as review of methods or techniques which have been used to address the problem of clouds in optical images.

iii. Chapter 3: This chapter outlines the methodology used for the study, the study area, data acquisition for the study, data pre-processing and how to define cloud both thin and thick. It also discusses how cloud shadow is defined or detected as well as how the detected clouds and cloud shadows were removed through interpolation technique.

iv. Chapter 4: This chapter discusses the results of every step in the methodology. The chapter presents results from detection of thick clouds, thin clouds and cloud shadow as well as the results from the interpolation technique used for cloud and cloud shadow removal.

v. Chapter 5: This chapter discusses the conclusions and recommendations of the study.

Chapter 2: Literature Review

2.1 Remote Sensing for Natural Resource Management

Remote sensing has successfully been applied in management of various natural resources both at global, regional and national scales. Researchers from the U.S. Geological Survey, University of Nebraska–Lincoln and the European Commission's Joint Research Centre, Ispra, Italy produced a 1 km resolution global land cover characteristics database for use in a wide range of continental-to global-scale environmental studies (Loveland, et al. 2010). The database was developed using unsupervised classification of Advanced Very High-Resolution Radiometer (AVHRR) images acquired through the period 1992-1993. Food and Agriculture Organization (FAO) has been carrying out global forest resources mapping using satellite images through their project named "FAO Global Forest Resources Assessment project" which is carried out in five-year cycle (Food and Agriculture Organization 2015). Additionally, FAO has also been mapping land cover at regional levels for establishment of land cover databases such as Africover and Asiacover projects which established land cover databases for the whole of Africa and Asia continents respectively.

Remote sensing has also been used for natural resources management at local scales, for example in Minnesota, it has been used for mapping and analysis of land and water resources using IKONOS and QuickBird images (Sawaya, et al. 2003) and in Turkey, forest mapping has been done using Landsat Images (Aydınm and Eker 2017). In Soviet Central Asia (Kazakhstan, Kyrgyzstan, Tajikistan, Turkmenistan, and Uzbekistan), remote sensing has been used for mapping of forests using Landsat and MODIS satellite images (Yin, et al. 2017) while in Congo, Synthetic Aperture Radar (SAR) has been used in mapping of forests in the Congo basin because of the ability of microwaves to penetrate all weather conditions (Cloud, Haze, Mist and Fog). In Kenya, remote sensing has successfully been used in mapping of water resources which produced Kenya Wetlands Atlas, a project that was undertaken by Ministry of Environment and Mineral Resources in collaboration with Department of Resource Surveys and Remote Sensing (DRSRS) (Ministry of Environment and Mineral Resources, Kenya 2012). Lastly, remote sensing has successfully been used in mapping of land cover in Kenya for the years 2000, 2010, and 2012-2014 which was required as an input for the System for Land Based Emission Estimation in Kenya (SLEEK) programme using Landsat satellite images. This project was accomplished by DRSRS in

collaboration with Regional Center for Mapping of Resources for Development (RCMRD), Kenya Forest Service (KFS) and Survey of Kenya (SoK).

2.2 Types of Earth Observation Remote Sensing Sensors

There are two primary types of sensors based on the source of energy that is used to illuminate the ground objects and they are active and passive sensors. Active sensors provide their own energy to illuminate the ground objects being remotely sensed while passive sensors do not produce their own energy but they rely on energy from the other sources majorly the sun. Examples of passive sensors are Accelerometer, Hyperspectral radiometer, Imaging radiometer, Radiometer, Sounder, Spectrometer and Spectroradiometer. Examples of active sensors are Laser altimeter, Lidar, Radar, Ranging Instrument, Scatterometer and Sounder. In this research, optical sensor which is an example of a passive sensor and Microwave sensor which falls under active sensors are used for data acquisition.

2.2.1 Optical Sensors

Optical Sensors detect the visible, near infrared and short-wave infrared wavelengths of the electromagnetic spectrum to form images of the earth's surface by recording the solar radiation reflected from targets on the ground (Aggarwal 2005). Land cover types reflect and absorb radiations differently at different wavelengths and this enables their differentiation. Some examples are outlined below;

i. **Panchromatic imaging system-** The sensor is a single channel detector sensitive to radiation within a broad wavelength range e.g. IKONOS PAN and SPOT HRV-PAN.

ii. **Multispectral imaging system:** The sensor is a multichannel detector with a few spectral bands. Each channel is sensitive to radiation within a narrow wavelength band e.g. LANDSAT MSS, LANDSAT TM., SPOT HRV-XS and IKONOS MS.

iii. **Superspectral Imaging Systems:** A Superspectral imaging sensor has many more spectral channels (typically >10) than a multispectral sensor e.g. MODIS and MERIS

iv. **Hyperspectral Imaging Systems:** A hyperspectral imaging system is also known as an "imaging spectrometer". it acquires images in about a hundred or more contiguous spectral bands e.g. Hyperion

2.2.2 Microwave Sensors

These are sensors that detect and record microwave portion of the electromagnetic spectrum that covers the range from approximately 1cm to 1m in wavelength. Compared to visible band, the microwaves have long wavelength and this property enables them to be of great importance in remote sensing. Longer wavelength microwave radiation can penetrate through cloud cover, haze, dust, and all but the heaviest rainfall as the longer wavelengths are not susceptible to atmospheric scattering which affects shorter optical wavelengths and this property allows detection of microwave energy under almost all weather and environmental conditions so that data can be collected at any time (Aggarwal 2005).

2.3 Challenges of Clouds using Optical Remote Sensing Satellites

The problem of clouds not only obstructs the ground but also cast their shadows on the ground hence impeding many applications of the optical images for remote sensing. Remote sensing satellites images have been used to monitor various phenomena on the surface of the earth such as land use change, land cover, floods, droughts, earthquakes and landslides and these applications are of great importance to humanity. Unfortunately, two thirds of the earth's surface is covered by clouds every year causing serious problems in optical remote sensing (Wang, et al. 1999). The International Satellite Cloud Climatology Project- Flux Data (ISCCP-FD) dataset estimates the global annual mean cloud cover is approximately 66% (Zhang, et al. 2004). Moreover, (Roy and Ju 2008) mentioned that Landsat-7 ETM+, one of the sources of optical satellite images, on average had about 35% cloud coverage in general. (Leckie 1990) found out that the probability of acquiring a cloud-free Landsat scene (cloud cover < 10%) can be as low as 10% for some regions in Canada. Therefore, it's quite clear that getting 100% cloud free optical satellite image is purely by luck. There are many varieties of clouds based on distance from the Equator but tropical environments are the cloudiest whereas the subtropics and the polar environments are 10%-20% less cloud (Candra, Phinn and Scarth 2016). Cloud heights in the tropical regions are much higher compared to those in other regions and they are approximately 1-2 kilometers higher than clouds in the mid-latitudes and more than 2 kilometers for clouds in the subtropics and polar regions. It is therefore for this reason that Kenya, an equatorial country is chosen for this study.

2.4 Status of Remote Sensing Technology in Africa

Africa comes very late in the field of remote sensing and spatial data infrastructures because it has no concrete means of possessing and creating satellite observation tools (Gerlinger 2013). One of the reasons is that Africa does not have any inter-governmental organization where resources can be pooled together for a specific purpose like in Europe where they have European Union. In 1979, the United Nations Economic Commission for Africa (UNECA) initiated five Remote Sensing Centers in the whole of African continent but to date, some of the centers are no longer functioning due to mismanagement and lack of funding. Out of the five centers, only three are functioning namely Remote Sensing Regional Centre of Ouagadougou (Burkina Faso), Regional Centre for Mapping of Resources for Development (RCMRD, Kenya) and Regional Centre for Training in Aerial Surveys (RECTAS) in Nigeria. Some African countries (Algeria, Nigeria, Egypt) have gained initial experience in building and/or operating remote-sensing satellites in cooperation with European countries and only South Africa has started building and operating its own satellites (Gerlinger 2013). South Africa's current goal is to develop, build and operate a transnational African remote-sensing system consisting of several small satellites by 2018 and Algeria, Kenya and Nigeria wish to be involved (Gerlinger 2013).

However, Kenya as a country has its own initiatives and has established a National Space Agency called "The Kenya Space Agency" through the signing by the president and gazettement of Kenya Space Agency order of 2017 (GoK 2017), the equivalent of National Aeronautics and Space Administration (NASA) of America. The Space Center is projected to cost the Kenyan tax payer ten billion Kenya shillings for a constellation of earth observation satellites and if successful will boost the country's security and provide solutions to challenges facing agriculture, education and medical sectors among others (Standard Media Group 2015). It will also have Kenya transition from a passive user of space and space technologies to a contributor to the development of space technology. Kenya's strategic location along the equator enables it exploit the ease of access to the equatorial orbits and particularly the geostationary orbits and the location of Indian Ocean to the East would facilitate ease of landing of space crafts as well as safe zone in case of unsuccessful launch.

Apart from the attempt by Kenya to create its own Space Center, there is already an existing Space Center called Broglio Space Center (BSC, San Marco Project), established in 1964 in Malindi through cooperation between Kenya and Italy Governments (Ibba 2007). The facility management

was under University of Roma “La Sapienza” up to the year 2004 after which the management was transferred to Italian Space Agency (ASI). The center consists of two segments, the Earth Segment and the Oceanic Segment. The oceanic segment represents the launch oceanic platform while the earth segment is the data reception center. In the last 40 years, the activities at the center range from rocket launches to satellite telemetry, tracking, and command (TTandC) support and remote sensing image acquisition. The number of launches from the center is twenty-seven (27), nine (9) of which are satellite launches with 100% success with the first launch done on march 1964 (Nike Apache) while the last launch was done in March 1988 (Scout Sv 206) (Ibba 2007).

2.5 ALOS Data

ALOS is an acronym which stands for Advanced Land Observing Satellite and it was launched in January 2006 by the Japan Aerospace Exploration Agency. Its Japanese name is “DAICHI” and it measures 3.5m wide, 4.5m long and 6.5m high and it uses solar battery and it has a gross weight of approximately four (4) tons which makes it one of the largest land observing satellites (Nguyen and Ryutaro 2009). ALOS has three sensors namely;

i. Panchromatic Remote-sensing Instrument for Stereo Mapping (PRISM), which is comprised of three sets of optical systems to measure precise land elevation.
ii. Advanced Visible and Near Infrared Radiometer type 2 (AVNIR-2), which observes what covers land surfaces and
iii. Phased Array Type L-band Synthetic Aperture Radar (PALSAR), which enables day-and-night and all-weather land observation.

ALOS general concepts are as outlined in *Table 2.1*

Table 2.1 General Concepts of ALOS Sensor

Sensor	***Spatial Resolution /Swath Width***	***Characteristics***	***Utilization***
PRISM	*Spatial Resolution: 2.5m* *Swath Width: 35km (Triplet mode)* *70km (Nadir Only)*	*It has three independent optical systems for viewing nadir, forward and backward producing a stereoscopic image along the satellite's track.*	*Cartography, making DSM for mapping, urban planning, agriculture, forest monitoring, coastal monitoring, monitoring illegal dumping, flood monitoring etc.*
AVNIR-2	*Spatial Resolution: 10m* *Swath Width: 70km*	*The Advanced Visible and Near Infrared Radiometer type 2 (AVNIR-2) is a visible and near infrared radiometer for observing land and coastal zones.*	*It provides better spatial land-coverage maps, wide range of urban planning, agriculture (vegetation research), forest monitoring, coastal monitoring, pollution monitoring on ports and harbors, plants monitoring, flood monitoring etc.*
PALSAR	*Spatial Resolution: 10m (fine resolution mode) 100m (Scan SAR mode) Observation Swath: 70km (fine mode) 250-350km (Scan SAR)*	*The Phased Array Type L-band Synthetic Aperture Radar (PALSAR) is an active microwave sensor using L-band frequency, which can observe with fine resolution in a conventional mode as well as wider swath with a SAR images.*	*It enables to make DEM, extract topography data by interferometry, estimate biomass, forest monitoring, agriculture, monitoring oil spill, moisture of soil, shipping inspection etc.*

The main Characteristics of ALOS satellite are shown in *Table 2.2*

Table 2.2 Major Characteristics of ALOS

Launch Date	*January 24, 2006*
Launching Vehicle	*H - IIA*
Launch Site	*Tanegashima Space Center, Japan*
Spacecraft Mass	*Approx. 4 tons*
Generated Power (Solar paddle)	*Approx. 7kw (at End of Life)*
Designed EOL (End of Life)	*3-5 years*
Orbit	*Sun Synchronous, Sub recurrent Repeat Cycle: 46 days Sub-Cycle: 2 days Altitude: 691.65km (Above the equator) Inclination: 98.16 deg.*
Attitude Determination Accuracy	*2.0 x 10-4 deg. (off-line, with GCP)*
Position Determination Accuracy	*1m (off-line)*
Data Rate	*240Mbps (Via Data Relay Test Satellite)* *120Mbps (Direct Transmission)*
On-board Data Recorder	*Solid-state Data Recorder (90Gbytes)*

The wavelengths of ALOS/AVNIR-2 bands are shown in *Table 2.3*

Table 2.3 Characteristics of ALOS AVNIR-2

Band	Wavelength (Nanometers)
1	4 2 0 – 5 0 0
2	5 2 0 – 6 0 0
3	6 1 0 – 6 9 0
4	7 6 0 – 8 9 0

2.6 Techniques used to address Clouds in Remote Sensing Data

Many approaches have been used for cloud and cloud shadow detection as well as their removal and these approaches can be grouped in to four categories;

i. Inpainting-based Approaches: In this approach, without use of multispectral and multitemporal data, regions contaminated by cloud and cloud shadow are reconstructed using inpainting techniques and image synthesis.
ii. Multispectral-based Approaches: In this approach, multispectral data is used for detection and removal of cloud and cloud shadow contaminated pixels. The different bands of the image are used to construct the cloud contaminated pixels.
iii. Multitemporal-based Approaches: This approach utilizes both temporal and spatial coherence to reconstruct the information missing from the cloud and cloud shadow contaminated pixels.
iv. Contamination detection approach: This approach uses either multispectral data or mathematical models to detect cloud and cloud shadows without proposing any approach for their removal in the images.

2.6.1 Multitemporal-based Approaches

The Multi-temporal based method is somewhat better method when compared to the Multi-spectral and in-painting method, it relies on both temporal and spatial coherence and has better ability to cope with large clouds (Ramya, KarthiPrem and Nithyasri 2014). Several researches have been done based on multitemporal approach and (Candra, Phinn and Scarth 2016) developed a Multi-Temporal Cloud Masking (MCM) algorithm which is based on multi-temporal satellite images of Landsat 8. The basic idea of this approach was to detect cloud and cloud shadow by using the difference reflectance values between clear pixels and cloud and cloud shadow contaminated pixels using two sets of images one with clouds and another one without clouds (Candra, Phinn and Scarth 2016). Band 3 and Band 4 were used for detecting cloud and non-cloud pixels whereas Band 5 and Band 6 are used for detecting cloud shadow pixels and non-cloud shadow pixels. According to the MCM, the accuracy assessment is very high and MCM approach can identify clouds to almost 100%. However, the drawback of this approach is that the assumption that very little or no change during between the acquisition dates of the two images may not hold especially when mapping or monitoring a highly changing geographical phenomenon. Secondly, Cloud and

Cloud Shadow Masking using Multi-Temporal Cloud Masking Algorithm is only able to detect thick clouds in optical images (Landsat 8 Images) and the problem of thin clouds in optical images still remains unresolved.

In another quest towards cloud free optical satellite images, (Wang, et al. 1999) presents another approach titled "Automated detection and removal of clouds and their shadows from Landsat TM Images". In this research, reflectance difference between cloud and non-cloud areas is used to detect cloud contaminated pixels and replace them with information acquired from cloud free multitemporal satellite images using image fusion technique. The cloud shadow areas are successfully detected by use of wavelet transform. After successfully detecting clouds and cloud shadow pixels, image fusion technique is used to replace information from cloud free image pixels to their corresponding cloud and cloud shadow contaminated pixels in the cloud image. The strength of this approach is that it has a lower computational complexity and it can successfully be used to detect and remove fog, haze, and mist from Landsat thematic mapper images. Nevertheless, this approach still has drawbacks and one of them is that the resulting fused image has some blocking artifacts which means the image would need further processing to make it useful for remote sensing applications. Again, accuracy assessment was not done for this approach which is a major gap because the user would like to know to what extent will the approach be able to remove clouds and cloud shadows so as to judge whether the algorithm will be useful depending on the intended use of the Landsat Thematic Mapper (TM) Images. Lastly, this approach needs further research with large number of images so as to get more precise threshold values for defining clouds and cloud shadows.

(Chao-Hung, et al. 2010) in their research "Cloud Removal from Multitemporal Satellite Images Using Information Cloning" also addressed the problem of clouds and cloud shadow in optical satellite images using Landsat-7 Enhanced Thematic Mapper Plus (ETM+) sensor images. The approach removes cloud-contaminated portions of a satellite image, and then reconstructs the information of missing data by utilizing temporal correlation of multitemporal images. The basic idea is to clone information from cloud-free patches to their corresponding cloud-contaminated patches under the assumption that land covers change insignificantly over a short period of (Chao-Hung, et al. 2010). Clouds are detected based on the fact that clouds are bright as well as cold in the thermal band and thresholding based technique is used to outline cloud extends/boundaries in the spectral temperature space. Once cloud boundaries have been outlined, cloud shadows are

identified roughly based on cloud location and solar illumination angle or direction. One strength of this approach is that it has the ability to process clouds from heterogeneous landscape and processes large amounts of cloud. However, this algorithm only detects thick clouds and the problem of thin clouds remains a challenge and it only proposes future plans to address the problem. This approach also cannot reconstruct information accurately for the cloud contaminated areas when the land cover changes significantly within a short time. The results presented by this approach also show that there is a slight discontinuity at the cloud contaminated boundaries even when smoothing operation is applied to these regions. Lastly, the manual refinement of cloud and cloud shadow using an interface needs further research for automation because it is tedious and time consuming.

Most high-resolution images have been distributed without an associated cloud mask and (Hagolle, et al. 2010) developed an algorithm called Multi-Temporal Cloud Detection (MTCD) for FORMOSAT-2 and LANDSAT images. This algorithm uses the blue wavelength to detect sudden reflectance increase on pixel by pixel basis and linear correlation tests based on pixel neighborhoods based on couple of images successfully acquired. Therefore, cloud detection criteria is guided by setting threshold values that define cloud using the blue spectral band. Computation of variations in order to detect cloud in an image requires cloud free reference image which is not always available and it has to be constructed from partly cloudy images. One strength of this algorithm is that it only uses blue band which all optical satellite data have and therefore this approach can be used for all optical satellite data (Candra, Phinn and Scarth 2016). However, this approach does not work well above inland water surfaces, which are prone to sudden variations of reflectance because of sunlight, turbidity or foam and water pixels must be discarded before computing the cloud mask (Hagolle, et al. 2010). Secondly, this algorithm does not detect thin clouds and high aerosols thicknesses and thin clouds may be confused as well with high aerosols thicknesses being regarded as clouds. Lastly, surface reflectance variations may occur as a result of agricultural activities such as cropping and ploughing or due to natural events like fires and snow covers or quick drying up of vegetation and when this occurs, rigorous processes are required to mask these activities so that they don’t end up being masked as cloud.

Closest Spectral Fit (CSF) method is presented by (Meng, et al. 2009) for cloud and cloud shadow removal from Landsat 5 Thematic Mapper images. The basic idea in Closest Spectral Fit (CSF) is to replace cloud and cloud shadow pixels with the most similar pixels from the cloud free areas in

the same image. In this approach, two images of the same area acquired at different times are used. The base image is the image with clouds and cloud shadows that requires masking and removal while the other image is called auxiliary image. In order for this CSF technique to work, cloud and cloud shadow areas in the base image should be cloud and cloud shadow free in the auxiliary image. Cloud and cloud shadows are detected based on the principle of sensitivity of visible and infrared bands to cloud and cloud shadows and for CSF, band 1 and band 3 are used for cloud detection while band 4 is used for cloud shadow detection and thresholds for defining both are derived. Once all the cloud and cloud shadow contaminated pixels are identified in the base image, their corresponding pixels in the auxiliary image are identified and their pixel values noted. The CSF algorithm then searches for the nearest pixels in the auxiliary image with the closest DN values and once identified, their corresponding pixels are identified in the base image. The identified base image pixel DN values are used to replace the cloud and cloud contaminated pixel and through such, clouds and cloud shadows are eliminated. One advantage of CSF is that accuracy of removing clouds and cloud shadows can be diagnostically checked when it is applied and statistical check of errors in predicting band values indicates whether this band could be used for further applications (Meng, et al. 2009). However, CSF has drawbacks and one of them is that this algorithm performs well for Landsat 5 Thematic Mapper but performs poorly when tested on Moderate Resolution Imaging Spectro-radiometer (MODIS) images.

In another attempt towards cloud free optical satellite images, (Stournara, Tsakiri-Strati and Patias 2013) presents another approach. In their study titled ‘Detection and removal of cloud and cloud shadow contamination from hyperspectral images of Hyperion sensor’, a scheme based on utilization of two multitemporal images one with clouds and another one without clouds for the same area is presented. In this study, cloud is detected based on the fact that reflectance values for clouds is much higher than the reflectance values of other pixels representing other land uses in the image. Similarly, reflectance values of cloud shadow pixels are relatively lower compared to other pixel values representing different land cover types within the image and therefore this characteristic enables discrimination of clouds and cloud shadow pixels from the rest of image pixels using thresholding. Generally, cloud removal based on multi-temporal images are known to yield better results but there is usually one drawback for all these approaches with regard to temporal resolution. Therefore, one of the drawbacks of this approach is that a span of considerable time might have elapsed until a cloud free image is available especially for countries in the tropics

which have (10%-20%) more cloud cover that the polar regions (Candra, Phinn and Scarth 2016). As a result, this drawback makes this approach and any other which utilizes the concept of multi-temporal images unsuitable for monitoring of high changing geographical phenomena. The other drawback is that this approach cannot be generalized for all the satellite images (Sensors) because the threshold values for defining clouds and cloud shadows are not fixed and they are different from one satellite sensor to another. Lastly, although cloud and cloud shadow contaminated pixels are replaced, there is still evidence of outline boundary of the previous cloud shadow or cloud region.

A practical method that produces cloud and shadow masks by flexibly using spectral (blue, NIR, MIR, and thermal bands), temporal information from two-date imagery, and spatial relationship (size, distance, and direction) between cloud and corresponding shadow is presented by (Jin, et al. 2013). In this approach, the pair of images (Target and Reference Images) are geometrically corrected and their digital numbers converted to top of atmosphere reflectance and thermal bands of the two images are transformed to at sensor brightness. Landsat blue and thermal bands are used for cloud detection due to the fact that clouds are normally brighter in the blue band and colder than the surface of the land from which they obscure information. In detection of shadows, band 5 mid infrared (MIR) is used and cloud shadows are detected based on the fact that shadows are usually darker and colder than the surface of the earth which they obstruct (Irish 2000). This algorithm removes false shadows based on the assumption that cloud shadow cannot be bigger than the cloud itself, clouds and cloud shadows are related based on the cloud location and sensor sun geometry. Once the clouds and cloud shadows are masked out, back filling of missing information is done. Pixels having the same spectral values are likely to be of the same land-cover type, and those pixels will likely have similar spectral values on a different date if no significant environmental and land-cover changes have taken place (Chen, et al. 2011). One of the strengths of this approach is that it produces one of the highest user accuracy after assessment of the final inputs. However, the drawback is that its only applicable when the assumption that there is negligible change of phenomena between the time of acquisition of the target image and the reference image otherwise the algorithm will not work.

2.6.2 Multispectral-based Approaches

This approach uses the multispectral information contained in a single image to detect clouds and cloud shadows and their removal using information contained in the same image. In the study "Removal of Thin Clouds Using Cirrus and QA Bands of Landsat-8" by (Shen, et al. 2015), a multispectral approach for cloud removal is developed. In this study, an algorithm to remove thin cirrus clouds and alto-thin clouds of Landsat 8 was developed. Cloud detection here is done using the Quality Assurance (QA) band which provides information on the presence or absence of clouds in Landsat 8 and reflectance data of band 9 is used for removal of cirrus clouds from Landsat 8. (Gao, Goetz and Wiscombe 1993) established a linear relationship between the reflectance at 1380 nm ($\gamma 1380$) and cirrus effect on the reflectance of wavelengths from 400 to 1000 nm. In this study ($\gamma 1380$) can be approximated by reflectance of Band 9. Thus, after the removal of cirrus clouds, the surface reflectance, γ_λ at wavelength of λ is ($\gamma_\lambda = \gamma_\lambda - \gamma_c$) where γ_λ is the reflectance after atmosphere correction at wavelength λ (Shen, et al. 2015). The removal is separately applied for all the bands from band 1 to band 5 above using band 9. The remaining thin clouds are removed using the quality assurance (QA) band. This approach however has got several drawbacks with the first one being that the QA band data is used and the thermal infrared data is required to generate the QA band but majority of the current operational optical sensors don't have a single thermal infrared (TIR) band. Secondly, the success of the replacement is dependent on the ability of Band 6 and Band 7 to penetrate clouds and in the event of any doubt, this would make the replacement questionable. Thirdly, if the cloud-covered area is over a water surface or the cloud-free area is water, the replacement can be erroneous because water absorbs almost all the solar radiation in Bands 6 and 7 and lastly, the possible existence of cloud effects on Bands 6 and 7 are not considered (Yang, et al. 2015).

2.6.3 Contamination detection approach

In this approach, algorithms are developed purely for detecting clouds, cloud shadows and other optical images contaminants such as snow without attempting to remove the contaminants from the optical images. Markov Random Fields for automatic cloud/shadow detection on high resolution optical images was developed by (Hégarat-Mascle and André 2009). This study was based on physical properties of clouds and shadows that both are connex objects with same shape and area and their relationship is based on their relative locations. Clouds and cloud shadows are

detected by Markov Random Field (MRF) framework at two distinct levels where one MRF for connexity modelling is done over the pixel graph and for cloud and cloud shadow relationship modelling, another MRF is done over the graph of objects. Some of the strengths of this approach is that performance is good based on the tested databases (39 SPOT/HRV images database), reduced false alarm rates (relative to classical pixel level approaches) and lastly fast convergence (relatively to methods requiring global optimization) (Hégarat-Mascle and André 2009).

However, this approach has got some drawbacks and one of them is the assumption of priori knowledge of the objects number and interactions between the objects and practically, this has an implication of over-detection of clouds and their shadows initially which will definitely have an impact in the final result. In order to address this short coming, this study tried to compare its approach to an approach where the number of objects and relationships among objects are unknown at a priori namely the Marked Point Processes (MPP). The Marked Point Processes (MPP) also has another drawback in that it is much heavier with regard to optimization process and computational time. Moreover, since Marked Point Processes (MPP) utilizes the global optimization approach, it's a mandatory requirement for setting of the model parameters precisely whereas local optimization of Markov Random Field (MRF) demands avoidance of such fastidious process.

The trade-off in multitemporal cloud, cloud shadow, and snow screening between higher accuracy and the possibility of masking out land cover change is significant and in an attempt to solve this problem, a new algorithm designed specifically for change detection that employs many images called Tmask (multiTemporal mask) was developed by (Zhu and Woodcock 2014). This algorithm was specifically meant for automated cloud, cloud shadow and snow detection in Landsat 7 images. This algorithm has two steps, the first step is based on a single-date algorithm called Fmask (Function of mask) that initially screens most of the clouds, cloud shadows, and snow while the second step benefits from the extra temporal information from the remaining "clear" pixels and further improves the cloud, cloud shadow, and snow mask (Zhu and Woodcock 2014). Instead of using the blue band (Band 1) for cloud detection as many multitemporal algorithms do, Tmask uses the green band (Band 2) for detecting clouds and snow (Wang, et al. 1999). The advantage of green band is that its less frequently saturated and its sensitivity to atmospheric influences is much less. The choice of near infrared (NIR) band (band 4) for cloud shadow and snow separation is based on the fact that cloud shadows are darker in NIR band and snow is brighter in NIR band.

The short-wave infrared band (Band 5) is chosen to separate clouds and snow because clouds are brighter in this band while snow is darker. One of the strengths of this algorithm is that compared to Fmask, Tmask has most improvement in cloud shadow detection than Fmask. Again, the Tmask algorithm does not falsely identify changes in landcover as cloud, cloud shadow or snow because it has the capacity of modelling land cover change. The results of snow and cloud detection in Tmask are better than Fmask as well. However, Tmask has a drawback in that the assumption that there is no significant land cover change between the date of acquisition between the multitemporal images may not hold for a fast-changing physical phenomenon. (Irish 2000)

A scene average Automated Cloud-Cover Assessment (ACCA) algorithm by (Irish, et al. 2006) has also been used to define clouds in Landsat 7 Image scenes. The primary goal of the Landsat-7 (L7) mission was to populate the U.S. held Landsat data archive with seasonally refreshed, essentially cloud-free Enhanced Thematic Mapper Plus (ETM+) imagery of the Earth's landmasses (Irish 2000). To achieve this goal, the Landsat Project Science Office (LPSO) at NASA's Goddard Space Flight Center (GSFC) developed the Long-Term Acquisition Plan (LTAP), a mission-long imaging strategy designed to optimize the 250 scenes acquired each day by the ETM+ (Arvidson, Gasch and Goward 2001). One of the techniques employed by LTAP was to use cloud cover reports from the Landsat 7 scene images already acquired for image acquisition scheduling by mission planners and it is for this reason that ACCA was developed purposely to provide cloud cover reports. Landsat 7 scenes ACCA algorithm uses visible, near infrared (NIR), shortwave infrared (SWIR) and thermal infrared to mask cloud (Irish 2000). Despite the rigorous efforts used in development of this algorithm, some drawbacks still exist and one of them is that it cannot detect clouds at extreme latitudes and high illumination angles because of presence of snow in those areas (Irish 2000) which is falsely identified as clouds. Although this algorithm can be used to define clouds on most parts of the earth, ACCA also has another drawback in its inability to detect thin cirrus clouds owing to the simple reason that it lacks high thermal response. Lastly, the greatest drawback of ACCA is that it only detects clouds and cannot detect cloud shadows which also obstruct image details.

A new method called Fmask (Function of mask) for cloud and cloud shadow detection was developed by (Zhu and Woodcock 2011) for Landsat Thematic Mapper (TM) and Enhanced Thematic Mapper Plus (ETM+) images. Probability mask is used for computing the cloud mask as well as image based thresholds. Lapse rate, flood fill transformation and object matching all

combined are used for cloud shadow masking in Fmask. Landsat Top of Atmosphere (TOA) reflectance (Bands 1,2,3,4,5and7) and band 6 Brightness Temperature (BT) are used as inputs and Fmask first uses rules based on cloud physical properties to generate potential cloud and cloud shadow layer (Zhu and Woodcock 2011). Through utilization of flood fill transformation, Near InfraRed (NIR) band is used to acquire layer of potential cloud shadow. One interesting fact in Fmask is the fact that estimation of cloud shadow location is done by use of satellite sensor view angle, solar zenith angle, solar azimuth angle and the clouds relative height. The latest version of Fmask utilizes the presence of new cirrus band in Landsat 8 for more accurate detection of thin cirrus clouds (Zhu, Wang and Woodcock 2015). In comparison with ACCA, Fmask has better accuracy of overall cloud detection (96.4%) whereas ACCA has overall accuracy of (84. 8%). Additionally, this algorithm exhibits good performance in high latitudes, it accurately does separate shallow/turbid water from clouds and above all, it can detect thin clouds and their shadows which is a capability rarely found in many algorithms. Lastly, Fmask has the ability to mask out snow in addition to masking cloud and cloud shadows which is another ability not found in many cloud and cloud shadow removal algorithms. However, Fmask still has some drawbacks associated with it and one of them is that it is unable to detect cloud which is warm and thin. Secondly, in the process of cloud classification, Fmask classifies very bright and cold land as clouds which is not the case. Lastly, Fmask may fail to detect cloud and cloud shadow for images which have heterogeneous surface reflectance because it uses a scene-based threshold and applies the same threshold to whole pixels in the image (Candra, Phinn and Scarth 2016).

(Hughes and Hayes 2014) developed a novel algorithm to define and classify clouds called Spatial Procedures for Automated Removal of Cloud and Shadow (SPARCS). This algorithm was developed using Landsat images and the approach uses Neural Network Approach (NNA) to define cloud, cloud shadow, water, snow, ice and clear sky classes for each pixel in the Landsat image scenes used. SPARCS development was motivated by the need for efficient and reliable cloud and cloud shadow masking in a forest change detection application over highly heterogeneous land cover in the eastern U.S. because existing methods were either too computationally intensive or missed many clouds or cloud shadows, which were detected as change (Hughes and Hayes 2014). The neural networks were trained by use of Landsat scene images with clouds and cloud shadows defined by human operators at united states geological survey (USGS) and evaluation done using manually defined data. One of the strengths of this

approach is that it uses sun and sensor geometry to identify regions of potential cloud shadow which reduces the ambiguity of wetland, hill shade and other land cover features which might have the same spectral signatures from being classified as cloud shadows when they are not. In a comparison with Fmask, a high-quality cloud and cloud shadow classification algorithm currently available, SPARCS performs favorably, with substantially lower omission errors for cloud shadow (Hughes and Hayes 2014). Again, in SPARCS, a measure of uncertainty is provided for the outcome of its classification which can be utilized by other algorithms that might be in need of clear sky pixels and looking at the overall accuracy, it outperforms even other methods that operates in the same conditions/constraints with an accuracy of 98.8% against 95.3%. Additionally, the SPARCS is fully automated and does not need specification of new parameters for any new scenes that can be used as an input and classification of any Landsat scene is completed under five (5) minutes on a standard desktop computer. However, this approach has got one drawback that there is limited support for inclusion of spatial information as an input.

Automated cloud and cloud shadow identification algorithms designed for Landsat Thematic Mapper (TM) and Thematic Mapper Plus (ETM+) satellite images have greatly expanded the use of Earth observation data by providing a means of including only clear-view pixels in image analysis and efficient cloud-free compositing (Braaten, Cohen and Yang 2015). In an attempt to actualize these capabilities to multispectral scanner (MSS) image, (Braaten, Cohen and Yang 2015) introduces MSS Clearview-mask (MSS-cvm). In definition, MSS-cvm is an automated rule-based algorithm for identifying clouds, cloud shadows, and clear-view pixels in MSS imagery (Braaten, Cohen and Yang 2015). In this approach, Thermal Infrared Band (TIR) is of great importance because of its characteristic interaction with cold temperatures of the cloud in order to separate clouds from other similar bright and white landcover or land use type like barren land, bare sand soils and rocks. TIR data are also used to identify cloud shadows by cloud projection and dark object matching using cloud temperature and adiabatic lapse rate to estimate cloud height, which is more accurate than spectral tests alone (Zhu and Woodcock 2011). Cloud identification is based on brightness in Band1 (B1) and the normalized difference between B1 and B2 according to the spectral test equation. One of the strengths of this approach is its high accuracy in cloud shadow masking because of its use of the thermal band to estimate cloud height, which allows for a more precise estimate of cloud projection and that is why MSScvm has less commission and omission error for the cloud shadow class than Fmask algorithm (Braaten, Cohen and Yang 2015).

However, this approach has some drawbacks with one of them being the fact that compared to other cloud and cloud shadow detection algorithms, its accuracy is 2.6% less compared to the Fmask algorithm therefore it's not emerging as one of the most accurate algorithms. Moreover, MSScvm algorithms accurately captures thick clouds irrespective of land cover type but it erroneously captures very bright barren land cover type as clouds and therefore more research needs to be carried out in order to improve on this. This approach is only applicable for sensors with the Thermal Infrared (TIR) Band and therefore it cannot be used as a universal approach towards cloud and cloud shadow masking from optical images.

The Landsat free and open data policy (Zhu and Woodcock 2014) provided the opportunity to realize the full potential of Landsat's unparalleled record of Earth observation data and this is why a lot of research has been done with the usage of Landsat images. (Huang, et al. 2010) presents another approach in their research titled "Automated masking of cloud and cloud shadow for forest change analysis using Landsat images" using Landsat Thematic Mapper (TM) and Enhanced Thematic Mapper Plus (ETM+) Images. The detection of cloud in this approach is guided by the characteristic that the spectral reflectance of clouds is much higher compared to other land cover feature types and clouds are also cold in the thermal band. Therefore, based on this fact, threshold values are derived to define cloud boundaries so as to separate cloud from other non-cloud features in the spectral-temperature space. Once this is achieved, the defined cloud pixels are used to define cloud shadow geometrically and also using spectral characteristics. Geometrically, the projected cloud shadow pixels are defined using the location of cloud pixels, the height of the clouds and the solar illumination geometry. The heights of the clouds are determined by using the normal environmental lapse rate of 6.4^0 C Km^{-1} based on differences in temperature between a cloud pixel and adjacent surface air. This approach has several limitations and firstly, due to the fact that it requires forest pixels to define the cloud boundaries, it can only be applied in areas where forest exists so that forest pixels can be derived and further research is required to establish whether it can be used for areas having few or no forest pixels at all. Secondly, this algorithm masks snow as cloud owing to the simple reason that snow is bright and cold and also confuses shadow and water due to dark appearance of both in the MSS Landsat Images. Lastly, this algorithm cannot detect clouds, smoke and fogs at lower altitudes which might have the same warmth as surface air. Despite the drawbacks associated with this algorithm, one of its strengths is that although it was designed for use with the Landsat EM and EM+, it can be adopted for use with other images

acquired by other sensors such as Advanced Space borne Thermal Emission and Reflection Radiometer (ASTER) and MODIS because these images contain both thermal and spectral bands.

In Satellite pour l'Observation de la Terre 5 (SPOT5) high resolution geometrical imagery, clouds and many other land cover features have very similar reflectance properties in all the four available bands of SPOT5 (green, red, near-infrared and shortwave-infrared). However, (Fisher 2014) presented a study called SPOT cloud and shadow masking (SPOTCASM) which was the first cloud masking process specifically designed for SPOT5 high resolution geometrical imagery. SPOTCASM is build based on the approach by (Hégarat-Mascle and André 2009) but there are some new inclusions. Firstly, water bodies are masked out of the images before searching for clouds and cloud shadows, the search area for shadows is limited by the assumption that clouds are similar in heights, removal of small objects by filtering possible clouds and growing clouds and cloud shadow segments based on marker pixels using watershed-from-markers transform. This model has got some strengths one of them being the ability to detect majority of thick clouds and it works across many landscapes from semi-arid shrubland to agricultural and forested areas. However, there are some drawbacks one of them being the assumption that all the clouds in the input images are of same height might not be true although it seemed to work for the input images used in the study (2 of the 313 images invalidated this assumption). Again, thin clouds are completely omitted by this model due to their similarity in spectral properties with some ground features. Another drawback is that false positive clouds which expected cloud shadow pixels are out of image extent are impossible to get rid of them by cloud-shadow routine matching. Lastly the manual editing of cloud and cloud shadow masks take a lot of time and further research needs to be done to automate it.

Cloud and cloud shadow removal from Landsat 8 imagery by use of both spectral and geometrical properties after a super-pixel segmentation process is presented by (Kalkan and Maktav 2017). In this approach, spectral and geometric properties of cloud and cloud shadow are employed for their detection with complementation from use of thermal infrared channels of Landsat 8 imagery. Neighborhood relations too is employed for improvement of accuracy detections of cloud shadows in the areas around clouds. This study can be regarded as a simplified, modified, automated and segmentation based version of ACCA and Fmask methods (Kalkan and Maktav 2017). The cloud areas are defined by use of rule-set based classification in which the calibrated reflectance images

are subjected to using super-pixel segmentation. Once the cloud areas are defined, evaluation of spectral tests as well as neighborhood relations with cloud areas is carried out to define cloud shadows. Near infrared band (Band 5) and shortwave infrared (SWIR) are used for cloud detection because in these bands, clouds have high brightness values than the other landcover features which makes them easily distinguishable. Cloud shadows are discriminated from other features by dividing thermal channel to the multiplication of three bands based on information of low-temperature characteristic of cloud features on thermal infrared bands (Red*NIR*Blue/Thermal 2) (Kalkan and Maktav 2017) . One of the strengths of this algorithm is that the precision and recall rates is better than the Fmask for the four different sites used for these tests. Additionally, this algorithm shows higher accuracy for cloud shadow detection compared to Fmask because of its adoption of cloud geometry projection combined with cloud shadow index for detection of cloud shadows. Lastly, the computation work load is greatly reduced because of its adoption of super pixel approach. However, this approach has got one drawback that adding neighbor edges of cloud and cloud shadow classes by region growing may end up classifying non-cloud and non-cloud shadow pixels as cloud and cloud shadow pixels respectively.

A simple threshold based algorithm by (Ghosh, et al. 2012) was developed for cloud detection for tropical environment of Bangladesh and its adjacent areas based on National Oceanic and Atmospheric Administration Advanced Very High-Resolution Radiometer (NOAA - AVHRR) satellite time-series data. This algorithm was developed in three tests, and test 1 is based on reflectance of channel 1 on AVHRR images, test 2 is based on temperature of channel 4 on AVHRR images and test 3 involves both channel 1 and channel 4 data. Test 1 and Test 2 are used for detection of clouds while Test 3 is used for cloud shadow detection. According to this study, one drawback is that reference values of temperature and reflectance are dynamic with seasonal variations and this means this algorithm needs to be subjected for all seasons to obtain the reference values for each season. Additionally, based on the tests that this algorithm is subjected to for detection of clouds, there is underestimation and overestimation witnessed. Another drawback is that dynamic threshold test cannot detect very thin clouds and during the monsoon period, visual inspection shows that test 2 cannot detect most of the low altitude broken clouds. The identified strength for this algorithm is that it can detect all clouds with reasonable accuracy and this judgement is based on visual inspection.

2.6.4 Inpainting-based Approaches

A novel method to produce continuous cloud free Landsat images imagery using spatially and temporarily weighted regression (STWR) is presented by (Chen, et al. 2017). The approach proposed in this study makes good use of the cloud-free information of the Landsat image scenes used as input and then uses the STWR model for optimal integration of complimentary information from invariant similar pixels. Identification of cloud and cloud shadow pixel is the first step before application of this STWR model/algorithm is used. In this approach by (Chen, et al. 2017) object based cloud and cloud shadow detection called Fmask is employed which has been discussed as an independent algorithm for cloud and cloud shadow detection in this literature. Once the cloud and cloud shadow pixels are identified, the input image is refined in to separate clouds because post cloud removal is based on patch by patch processing. One of the strengths of this approach is that a complete framework for continuous cloud removal is provided and has a potential for use in the other optical images. Testing of the STWR model was done using both simulated and actual Landsat series of images and yields visually and quantitatively good results. However, one of the drawbacks of this approach is that the mutual difference resulting from atmospheric conditions and solar illumination are not considered which in an ideal situation it should. Secondly, this approach lacks the ability to restore accurate information in the event of landcover change occurrence.

Therefore, in an effort to build on these developments, and to further enhance usability of optical remote sensing images by cloud and cloud shadow removal, this research presents a completely different approach which combines optical and microwave data for cloud and cloud shadow removal through interpolation technique. A step by step approach on development of this algorithm is as outlined in the next chapter on methodology.

Chapter 3: Methodology

The methodology used in this research is as outlined in *Figure 1.1* and it gives an overview of how data from Advanced Land Observation Satellite (ALOS) was used in development of cloud and cloud shadow removal algorithm. In this study, the Advanced Visible and Near Infrared Radiometer type 2 (AVNIR-2) was used as the source of the optical image and Phased Array L-band Synthetic Aperture Radar (ALOS/PALSAR) image was used for the microwave data. Cloud is always a problem in optical images and ALOS/AVNIR-2 being an optical image is not spared either but ALOS/PALSAR is not affected due to the ability of microwaves to penetrate clouds, haze, fog and other bad weather conditions. In this study, clouds are removed from optical images (ALOS/AVNIR-2) based on interpolation technique from microwave data (ALOS/PALSAR). Clouds are defined by use of two indices namely Total Reflectance Radiance Index (TRRI) and Cloud Soil Index (CSI). TRRI is an index developed by Professor Nguyen Dihn Duong and CSI is an index developed by Nguyen Thanh Hoan based on studies he had carried out before (Nguyen and Ryutaro 2009). This approach works best when the optical image and the microwave image acquisition date is not far apart and with ALOS this condition is fulfilled perfectly because the optical sensor and the microwave sensor are onboard in the same imaging platform. Cloud shadow is later defined by projecting the defined clouds using average distance and bearing derived from measurements carried out between sampled clouds and their corresponding shadows.

3.1 Study Area

The study area measures forty-five Kilometers (45 Km) by twenty-five Kilometers (25Km) polygon and geographically it cuts across Bomet, Narok and Nakuru Counties. It also cuts across Maasai Mau, Transmara, Olpusmoru, Eastern Mau and South West Mau forests which form part of one of Kenya's water tower, the Mau forest complex. This is as shown in *Figure 3.2.* Universal Transverse Mercator (UTM) zone 37S based on WGS84 datum coordinate system was used for the study area map and using coordinates, the study area rectangle is defined by top left corner (781556.699m,9945201.99m) and bottom right corner (826556.69m,9920201.99m). The study area linked with the acquired cloud image is as shown in *Figure 3.3*

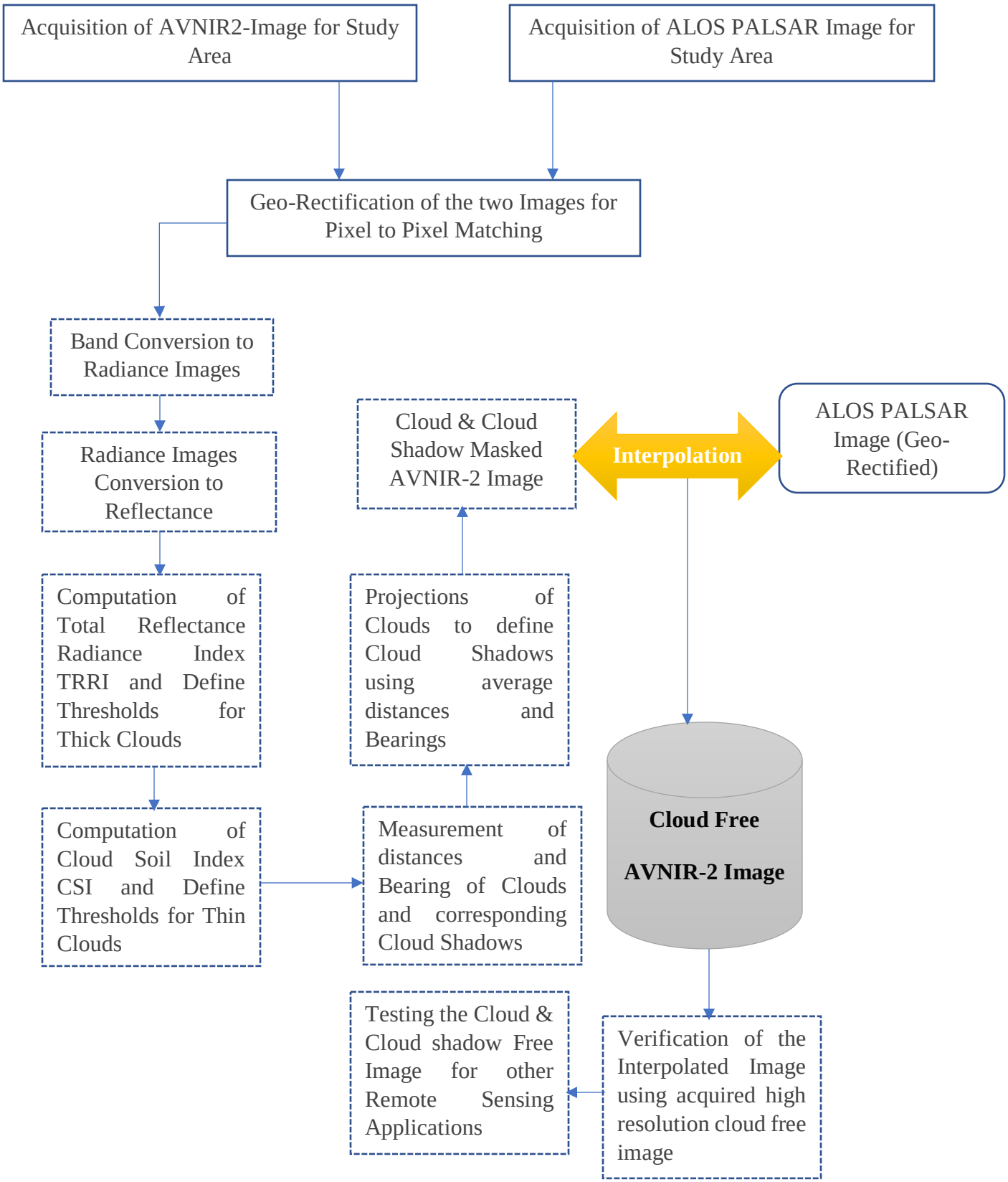

Figure 3.1 Flow Chart of Methodology

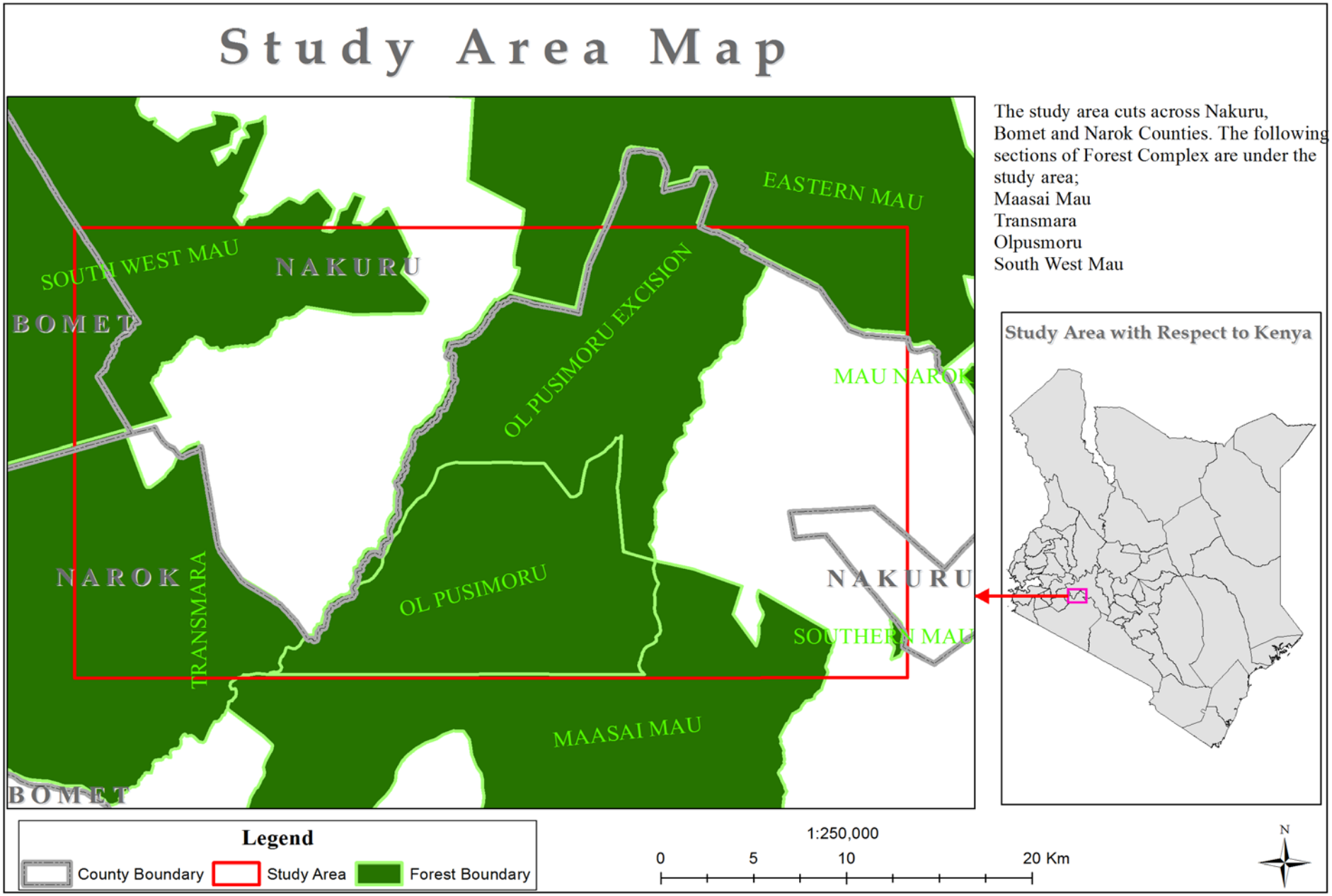

Figure 3.2 Study Area Map

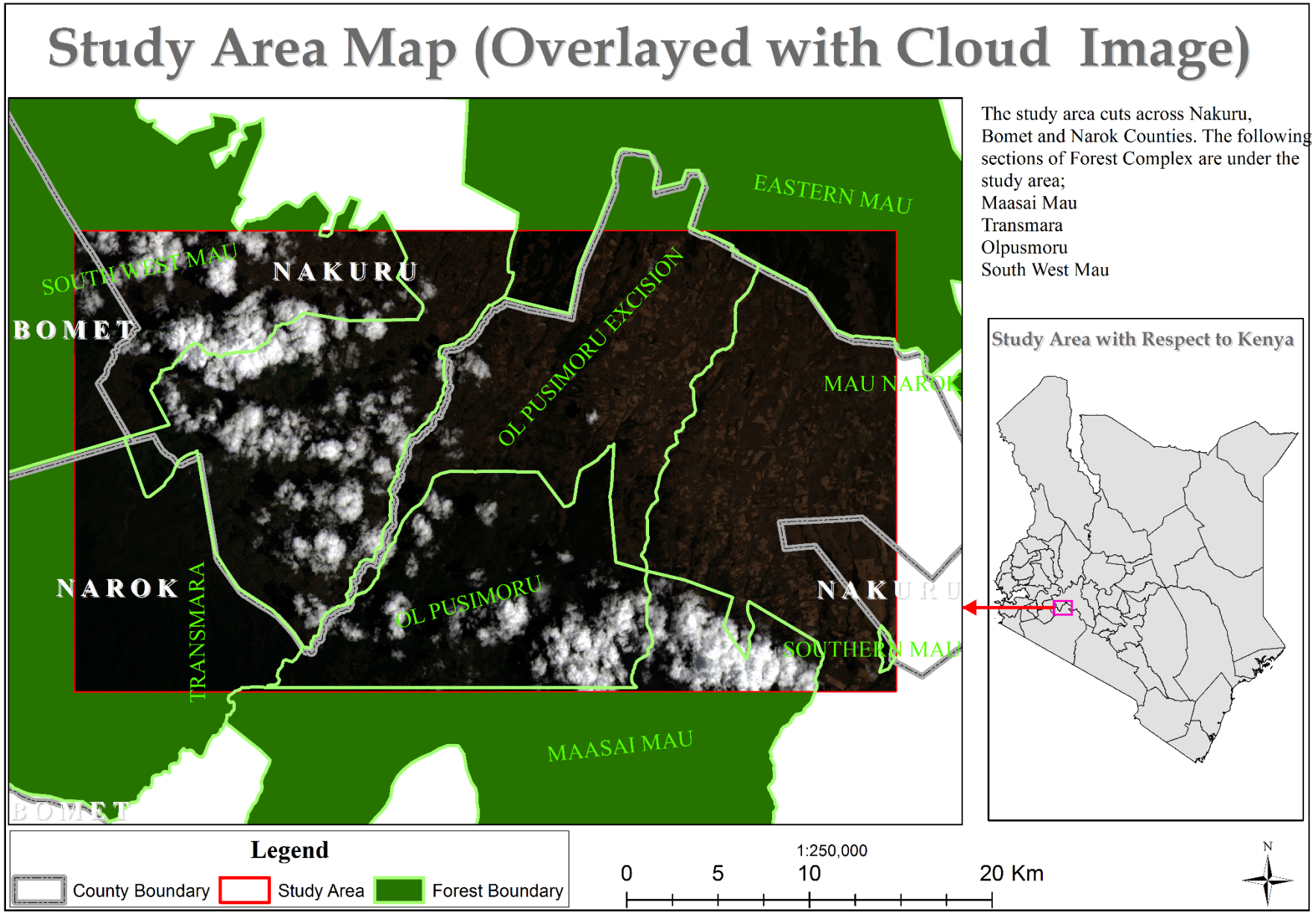

Figure 3.3: Study Area Linked with Image

3.2 Data Acquisition

In this study AVNIR-2 optical image and ALOS PALSAR image for the study area were purchased from Remote Sensing Technology (RESTEC) center of Japan. They are as shown below.

Plate 3.1 AVNIR-2 Image

Plate 3.2 ALOS PALSAR Image

The acquired images had been projected to Universal Transverse Mercator (UTM) zone 37 South using WGS 84 datum and the coordinate system was maintained for subsequent project processes.

3.3 Data Pre-processing

The acquired data could not be used as it was and data pre-processing was carried out to both the radar and optical image. The following data processing activities were carried out.

3.3.1 Geo-Rectification

The AVNIR-2 Image and the Radar (ALOS PALSAR) image were not overlaying correctly when loaded and viewed in ArcGIS. This was noted by non-overlaying of similar features in both sets of images as observed in ArcMap and geo-rectification was done. Geo-Rectification was done using image registration by use of similar features which appeared in both the Radar (ALOS PALSAR) and optical (AVNIR-2) images. The rectified images were then resampled to pixel size of ten by ten meters and snapping was done during resampling to ensure pixel to pixel matching in both images.

3.3.2 Radiance and Reflectance Conversion

In the computation of Total Reflectance Radiance Index (TRRI), the input bands information is usually calibrated image values which is reflectance. In order to process image reflectance, the image radiance was first computed because radiance is used as an input in computation of reflectance and this was done for all the AVNIR-2 image bands. This was done using MATLAB and the following formula was used.

$$L_\lambda = DN*Gain + Offset \qquad (3.1)$$

Where;

L_λ = Radiance

DN = Digital Number

Gain = Band Multiplication Factor

Offset = Band Additive Factor

The digital number is usually the pixel values of the image while the gain and offset values for each band was contained in the image header file and are as shown in *Table 3.1*

Table 3.1 Band Gain and Offset for AVNIR-2 Image

Band	Gain	Offset
Band 1	0.5880	0.000
Band 2	0.5730	0.000
Band 3	0.5020	0.000
Band 4	0.5570	0.000

Gains and offsets are in units W/ (m2 * sr * µm) and therefore radiance will be in units of W/ (m2 * sr * µm). Reflectance was computed using the following formula for all the bands;

$$\rho_\lambda = \pi L_\lambda d^2 / ESUN_\lambda Sin\Theta \qquad (3.2)$$

Where;

L_λ = Radiance in units of W/ (m2 * sr * µm)

d = Earth-sun distance, in astronomical units.

$ESUN_\lambda$ = Solar irradiance in units of W/ (m2 * µm)

Θ = Sun elevation in degrees

The parameter L_λ is computed in $L_\lambda = DN*Gain + Offset$ while π, d, $ESUN_\lambda$ and Θ are provided in the metadata header file. This is as shown in *Table 3.2*

Table 3.2 Reflectance Computation Parameters

Parameter	Value
d	1.0103742
$ESUN_\lambda$	B1=1943.3, B2=1813.7, B3=1562.3 B4=1076.5
Θ	65.20

3.4 Cloud and Cloud Shadow Definition

Thick Cloud is defined using the TRRI using the defined thresholds while thin cloud is defined using the CSI using the defined thresholds as well. Cloud shadow is defined by projecting the

defined clouds using bearings and distances measured from a sample of the defined cloud patches. A detailed discussion of each is as shown in the following sub-sections.

3.4.1 Thick Cloud

The ALOS/AVNIR-2 image is a four-band image with spatial resolution of ten (10m) meters (Japan Aerospace Exploration Agency, 2016) and the wavelengths are as outlined in *Table 3.3*

Table 3.3 AVNIR-2 Image Bands Wavelengths

Band	Wavelength (micrometers)
Band 1	0.42 to 0.50
Band 2	0.52 to 0.60
Band 3	0.61 to 0.69
Band 4	0.76 to 0.89

The reflectance of clouds is always high from visible bands to near infrared bands of the electromagnetic spectrum and therefore the reflectance values of clouds will be high in all the four (4) bands of ALOS/AVNIR-2 image. As a result, thick clouds were defined by the TRRI index which is defined by the following formula;

$$TRRI = \frac{\int_1^n I_i \, \Delta}{\int_1^n I_{max} \, \Delta} * 100 \qquad (3.3)$$

Where: TRRI = Value of Index;

I_i = Digital count of channel I;

n = Number of spectral channels;

I_{max}= Maximum digital count

Δ= Spectral channel difference

In other words, TRRI as defined by the above formula is the area under the spectral reflectance curve which is then expressed as a percentage. Using reflectance, it is simplified as;

TRRI*= (B1+ {2*(B2+B3)} +B4)/2) *100* *(3.4)*

Using the TRRI index computed, any pixel whose TRRI Index is greater 60% is considered a cloud pixel. The TRRI image is as shown in *Plate 3.3*.

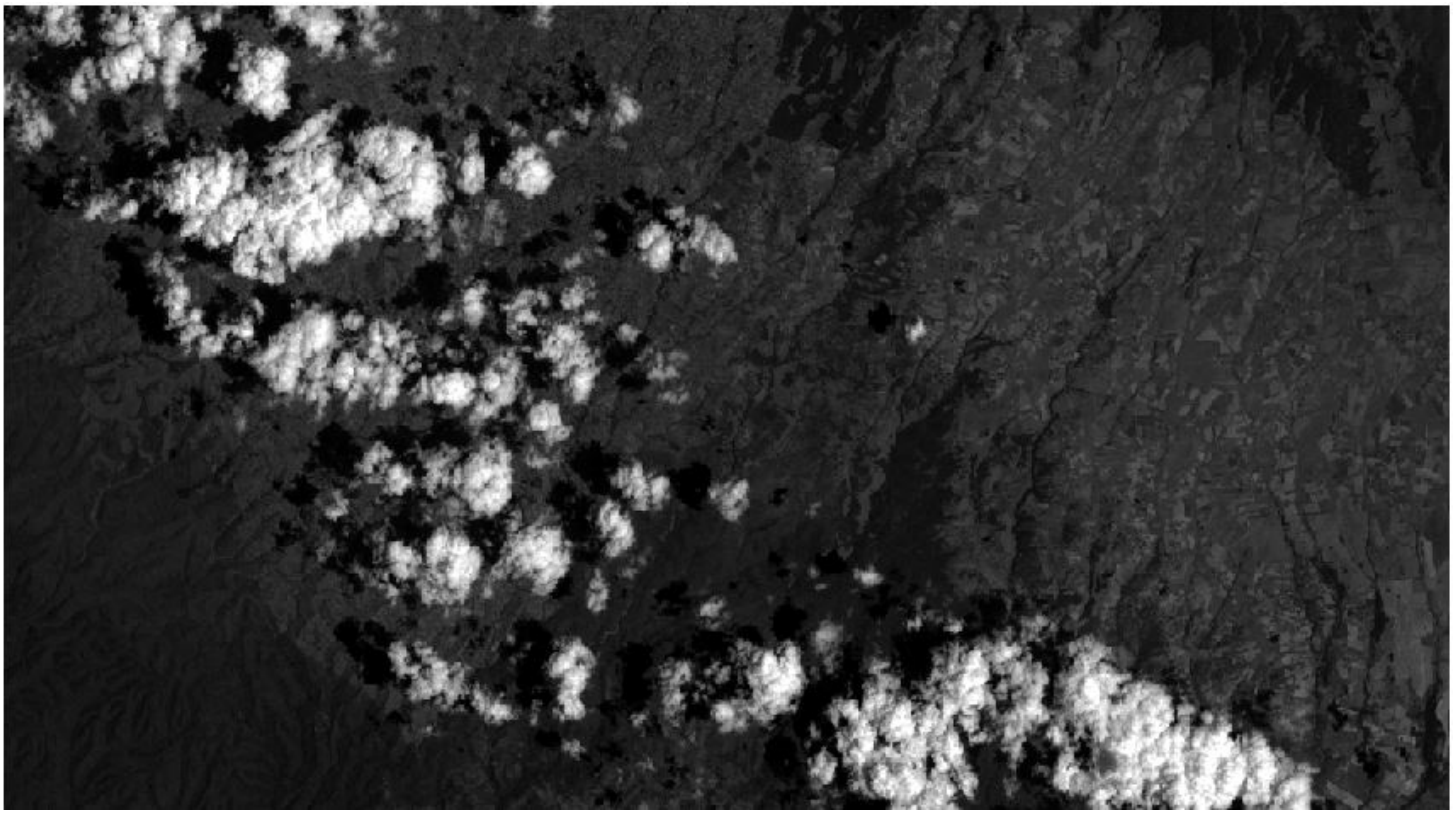

Plate 3.3: TRRI Index Image

3.4.2 Thin Cloud

Thin clouds are usually more difficult to define because they have some similarities with some land cover types like dry sand or dry barren soil. However, from visual to infrared wavelength, reflectance of dry barren land is always increasing as per increasing wavelength whereas for water it always dips. In the mixture part between clouds and dry barren land or dry sand, reflectance of thin cloud in blue band (band 1) is higher than that of dry soil and reflectance of thin cloud in band 4 is lower than that of dry soil and therefore thin cloud and other dry objects can be separated by Cloud -Soil Index (CSI) (Nguyen and Ryutaro, 2009). This index is calculated as follows:

$$CSI = \frac{Band\ 1 - Band\ 4}{Band\ 1 + Band\ 4} \qquad (3.5)$$

Using the CSI index, any pixel whose CSI index is greater than -0.30 and less than -0.20 is considered a thin cloud pixel. The resulting CSI index image is as shown *Plate 3.4*.

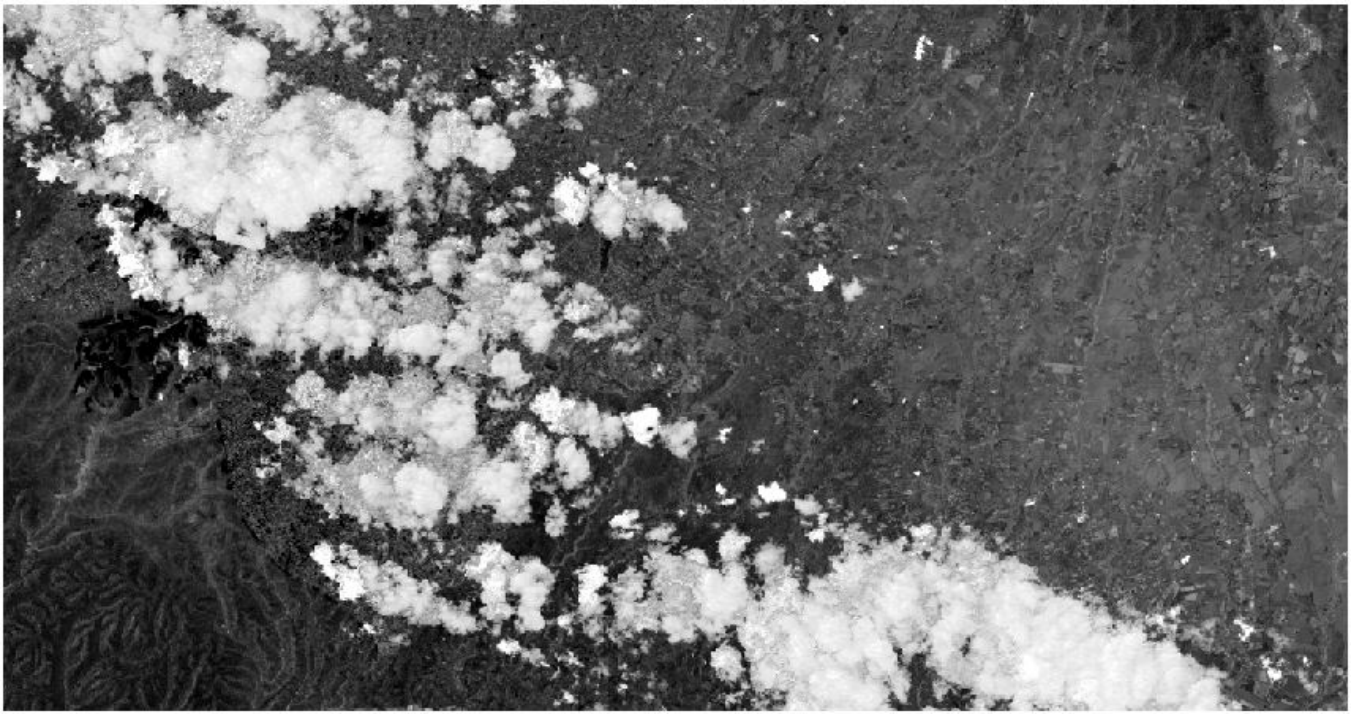

Plate 3.4: CSI Index Image

3.4.3 Cloud Shadow

Defining cloud shadows in this research was based on the assumption that clouds and their cloud shadows are similar in area and therefore to define cloud shadows, average distances and bearings of clouds to their corresponding shadows was measured for a sample of clouds patches. The average of distances and bearings measured was computed and these averages were used to project cloud shadows from the already defined clouds. Clouds are usually at different height and the assumption made here is that clouds are at the same height, but this results in under and over detections of clouds. To address this, the average under detection was used to grow the cloud shadow areas so as to ensure all the cloud shadows are captured. The average distance and bearing from clouds to their corresponding shadows are as shown in *Table 3.4*

Table 3.4 Average Distance and Bearing to Cloud Shadows

Cloud Patch	Distance to Shadow (M)	Bearing (Degrees)
Patch 1	762.851	238.184198
Patch 2	736.348	240.095521
Patch 3	763.205	243.212873
Patch 4	878.703	239.960885
Patch 5	917.753	242.437638
Patch 6	968.726	237.039112
Average	**837.931**	**240.1550378**

3.5 Developing Algorithm for Cloud Removal

Development of the algorithm started from detection and masking of cloud and cloud shadow contaminated pixels in the optical satellite image. Thick clouds were detected using TRRI while thin clouds were detected using CSI. The defined thresholds for TRRI and CSI were used to mask out thick and thin cloud contaminated pixels respectively. Cloud shadows were detected by projecting the detected clouds using the average of measured distances and bearings of sampled cloud patches to their corresponding cloud shadows. In order to remove cloud and cloud shadow contaminated pixels from the cloud image, interpolation technique was used. For every cloud and cloud shadow contaminated pixel in the optical cloud image, their corresponding pixels in the radar image were identified. The identified pixel values in the radar image were then used to search for the nearest pixels with similar or closest pixel value and once identified, their corresponding pixels were identified in the optical image and these pixel values in the optical image were used to replace pixel values for the cloud and cloud shadow contaminated pixels. This concept is based on the first law of geography which states that "everything is related to everything else, but near things are more related than distant things" and this is why the search is done inward out from the pixels as shown in *Figure 3.4*. This was done using MATLAB programming language starting from the detection of thick clouds, thin clouds and cloud shadow as well as the use of interpolation technique for cloud and cloud shadow removal.

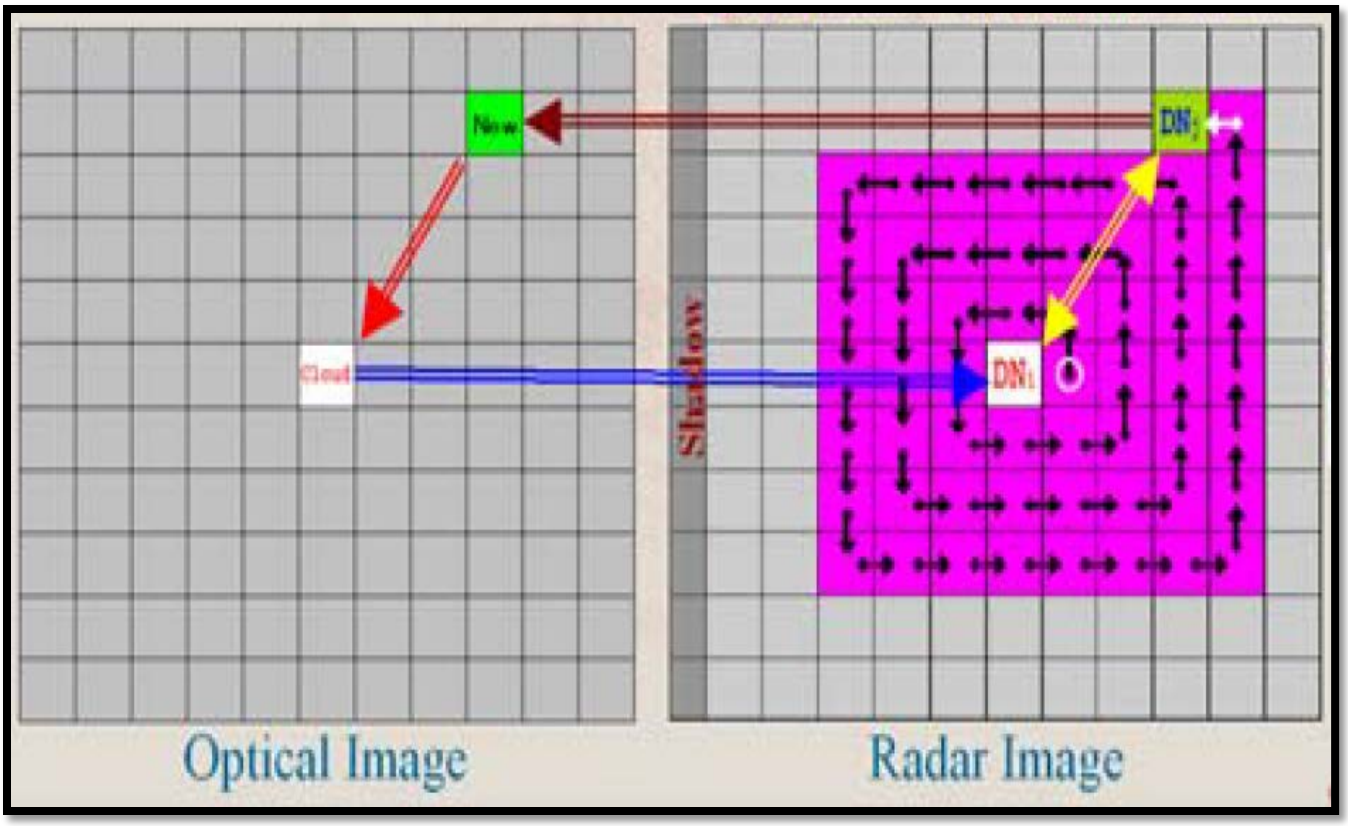

Figure 3.4 Interpolation Technique for Cloud Removal

3.6 Testing the Algorithm

The developed algorithm was tested using the acquired data in order to assess its performance with regard to cloud and cloud shadow detection and removal. The input datasets were the cloud contaminated image and the radar image which were required for cloud and cloud shadow detection and removal using interpolation technique.

3.7 Application of the Cloud and Shadow Free Image for Land Cover Analysis

The cloud and cloud shadow free optical satellite image resulting from the cloud removal algorithm was subjected to land cover analysis to test its suitability for land cover mapping. This was meant to assess the usefulness of the resulting cloud free optical image for other remote sensing applications.

Chapter 4: Results and Discussions

This chapter presents the results of the algorithm and discussions of the results. This is as discussed in the subsequent sections based on the methodology described in Chapter three.

4.1 Identified Clouds and Cloud Shadows

Thick clouds were defined using Total Reflectance Radiance Index (TRRI) while thin clouds were defined using Cloud Soil Index (CSI) thresholds as defined in the methodology. The detection and masking of each is as discussed in the following subsections.

4.1.1 Thick Clouds Masked.

The detection of thick clouds was done using Total Reflectance Radiance Index (TRRI) and based on the defined thresholds (TRRI>=60%), the thick clouds were masked out of the AVNIR-2 image. This is as shown *Plate 4.1* where yellow areas are the thick cloud areas in the optical satellite image.

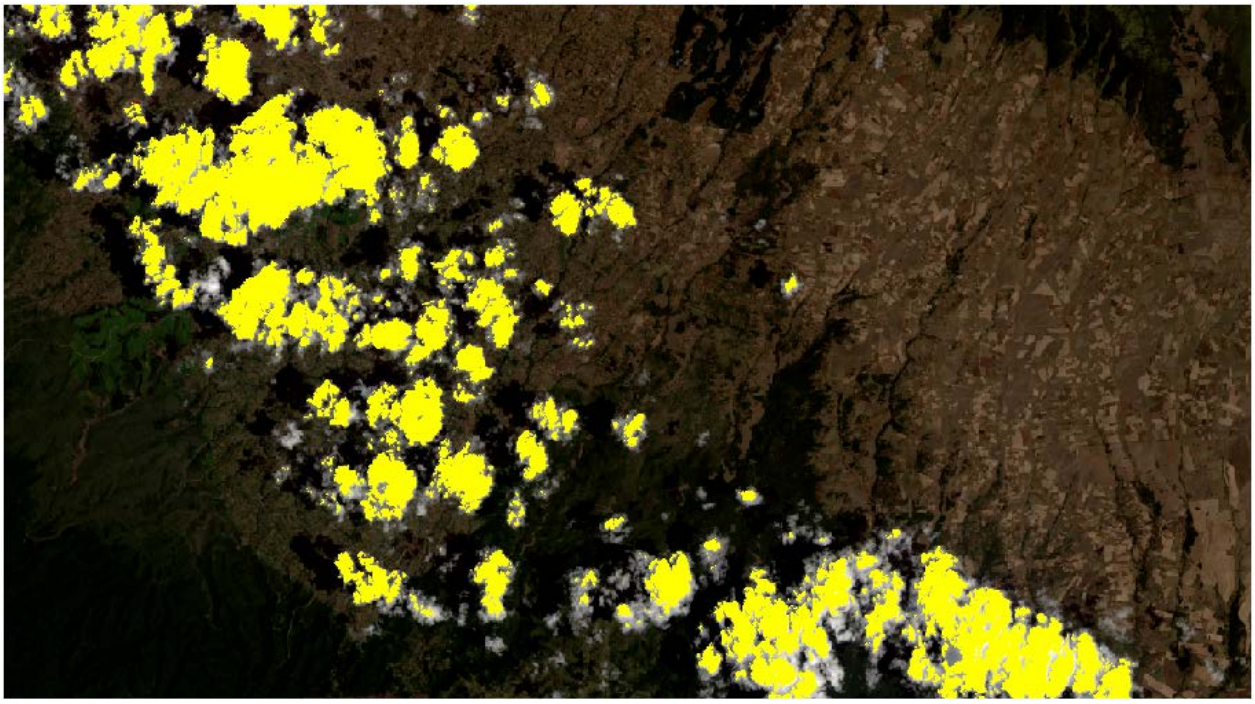

Plate 4.1: AVNIR-2 Image Thick Clouds Masked

The thick clouds as observed above cuts diagonally across the image with their distribution occurring both over forest and farmland and obscuring details there under together with their corresponding clouds. Visual examination shows that thick clouds are well masked out using the

Total Reflection Radiance Index (TRRI) without any omissions and the results are quite impressive.

4.1.2 Thin Clouds Masked.

Detection of thin clouds was done using Cloud Soil Index defined thresholds (-0.3<CSI<-0.2). Any pixel whose cloud soil index was between the defined range was defined as a thin cloud pixel and therefore masked out from the AVNIR-2 image. This is as shown in *Plate 4.2* where thick clouds are the yellow areas and thin clouds are the red areas.

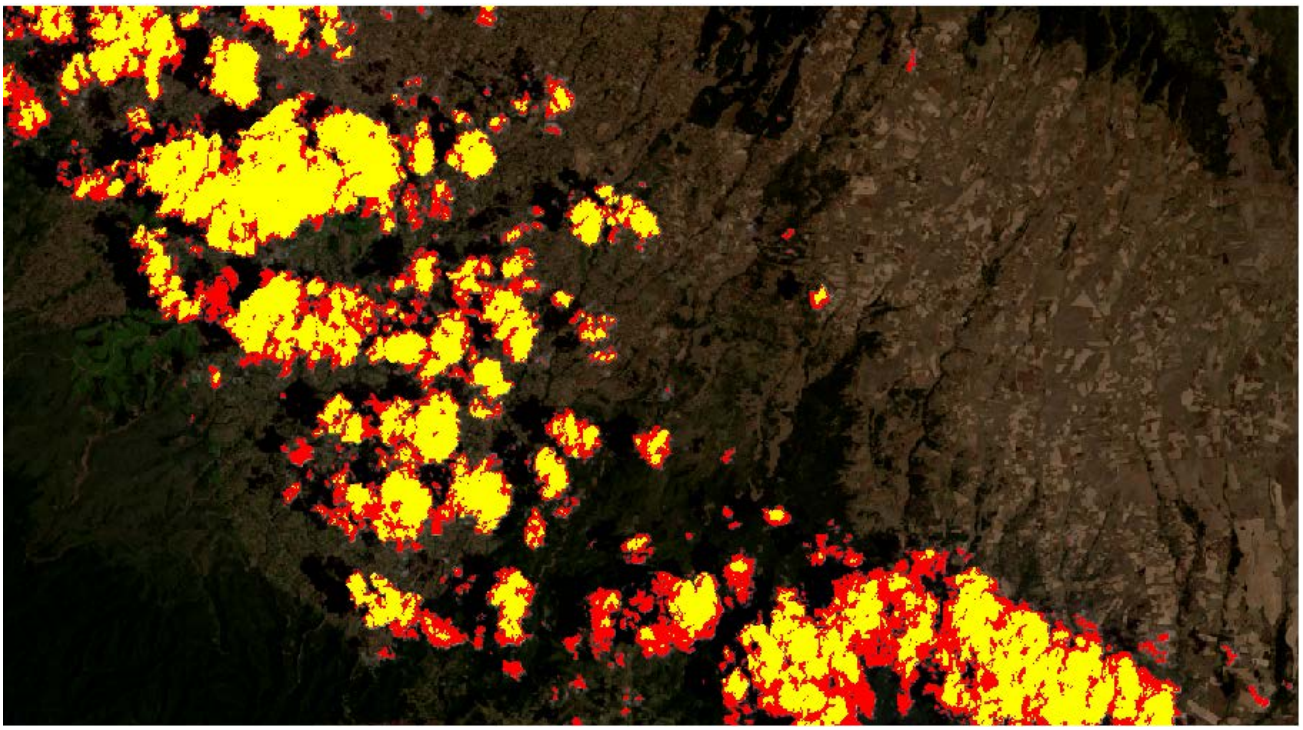

Plate 4.2: AVNIR-2 Image with Thin Clouds Masked

As it is observed above, most of the thin clouds are occurring around the thick clouds because the intensity of thick clouds decreases as you move to the edges hence forming thin clouds around the thick ones. Again, visual examination shows that there still remain patches of undetected thin clouds both around the thick clouds and isolated standalone patches which still obscure image information below them. Therefore, as CSI is used to detect thin clouds, there remains a considerable amount that remains undetected and they still obscure image information below them.

4.1.3 Cloud Shadows Masked

Masking of cloud shadow was done by projecting the already defined thick and thin clouds based on the average distances and bearings measured from a sample of the cloud patches in the optical satellite image. The red color shows projected cloud shadows while the yellow color depicts both thin and thick clouds as shown in *Plate 4.3*.

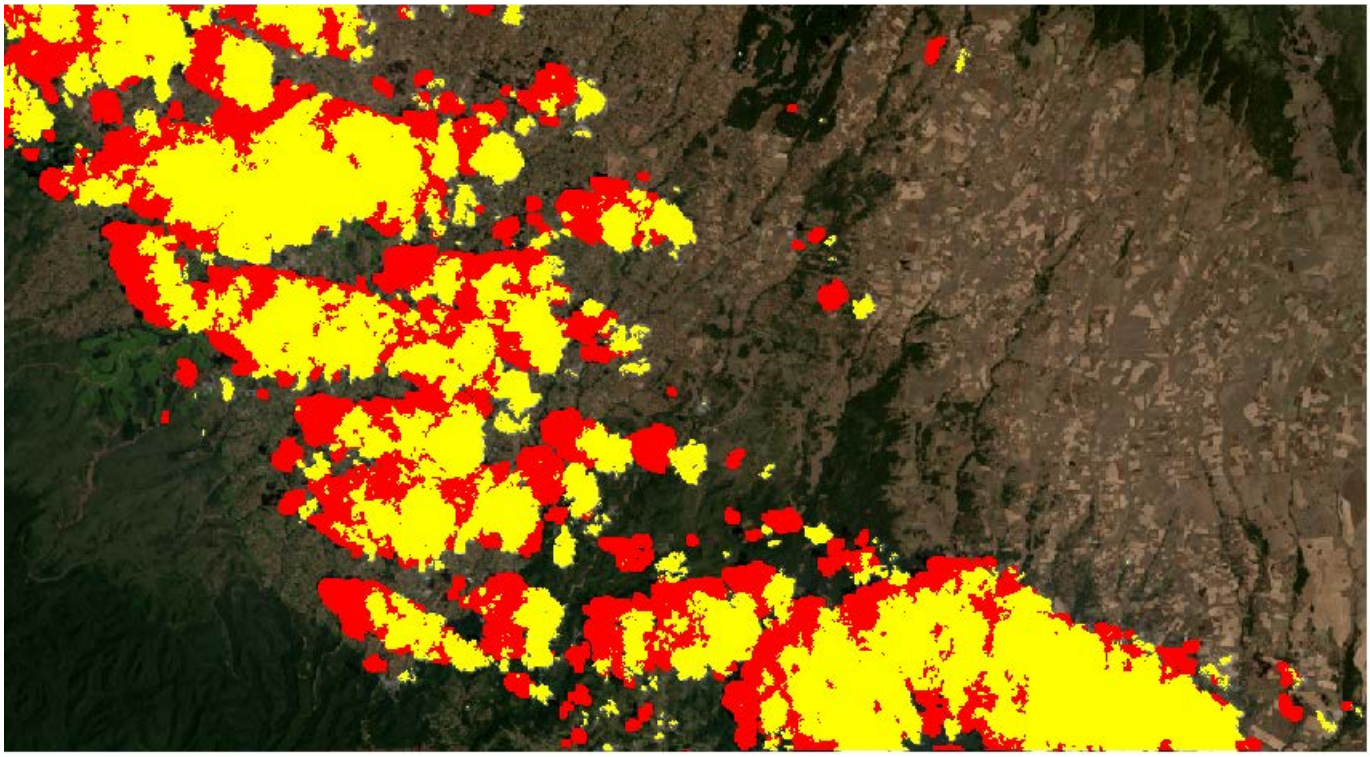

Plate 4.3: Cloud Shadow Mask

As shown above, visual observation shows that all the cloud shadows are occurring to the west of their corresponding cloud meaning that the image was taken in the morning hours and the cloud shadow detection approach used captured most of the cloud shadows. However, it should be noted that the regional growth of cloud shadows around their area of occurrence by using the average of the under-detection distance is what enabled good capture of the cloud shadows and to some extend covered the thin clouds patches which were occurring around the thick clouds. This approach however good it is in capture of undetected cloud shadow has the negative effect of increasing the computational effort required during interpolation to remove the cloud shadows in areas captured as cloud shadows when they are not.

4.1.4 Cloud and Cloud Shadow Masking combined

The masking of both cloud and cloud shadow was done for the AVNIR-2 image and this is as shown in *Plate 4.4* where the dark areas are the masked areas. Visual observations show that the combined thick and thin clouds and their corresponding shadows were well masked out of the image but close observation shows that the thin clouds are still present in the image because as discussed in the thin clouds masking, there were some thin clouds which went undetected and that is why they are still present. Thin clouds therefore are a challenge and need rigorous detection approach for effective masking. The image which has been masked from cloud and cloud shadow contaminated pixels is as shown in *Plate 4.5* linked with the study area.

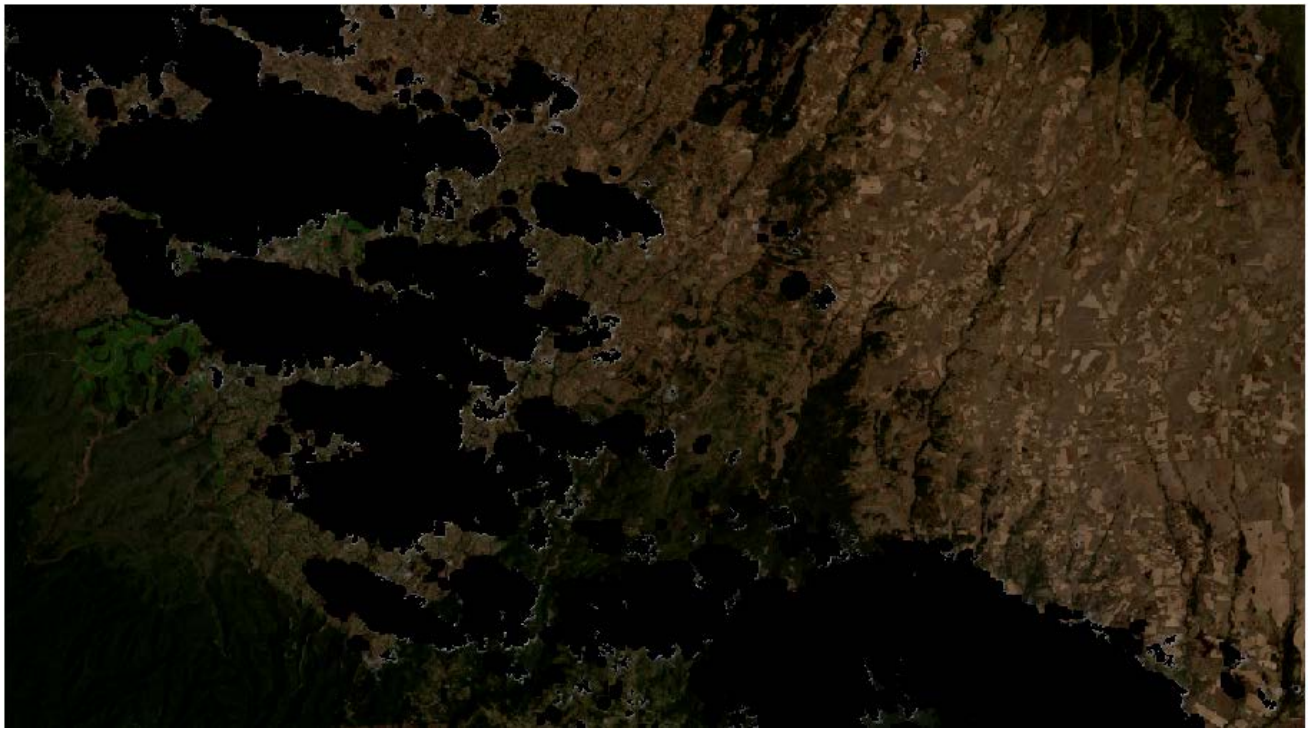

Plate 4.4: Cloud and Cloud Shadow Masked

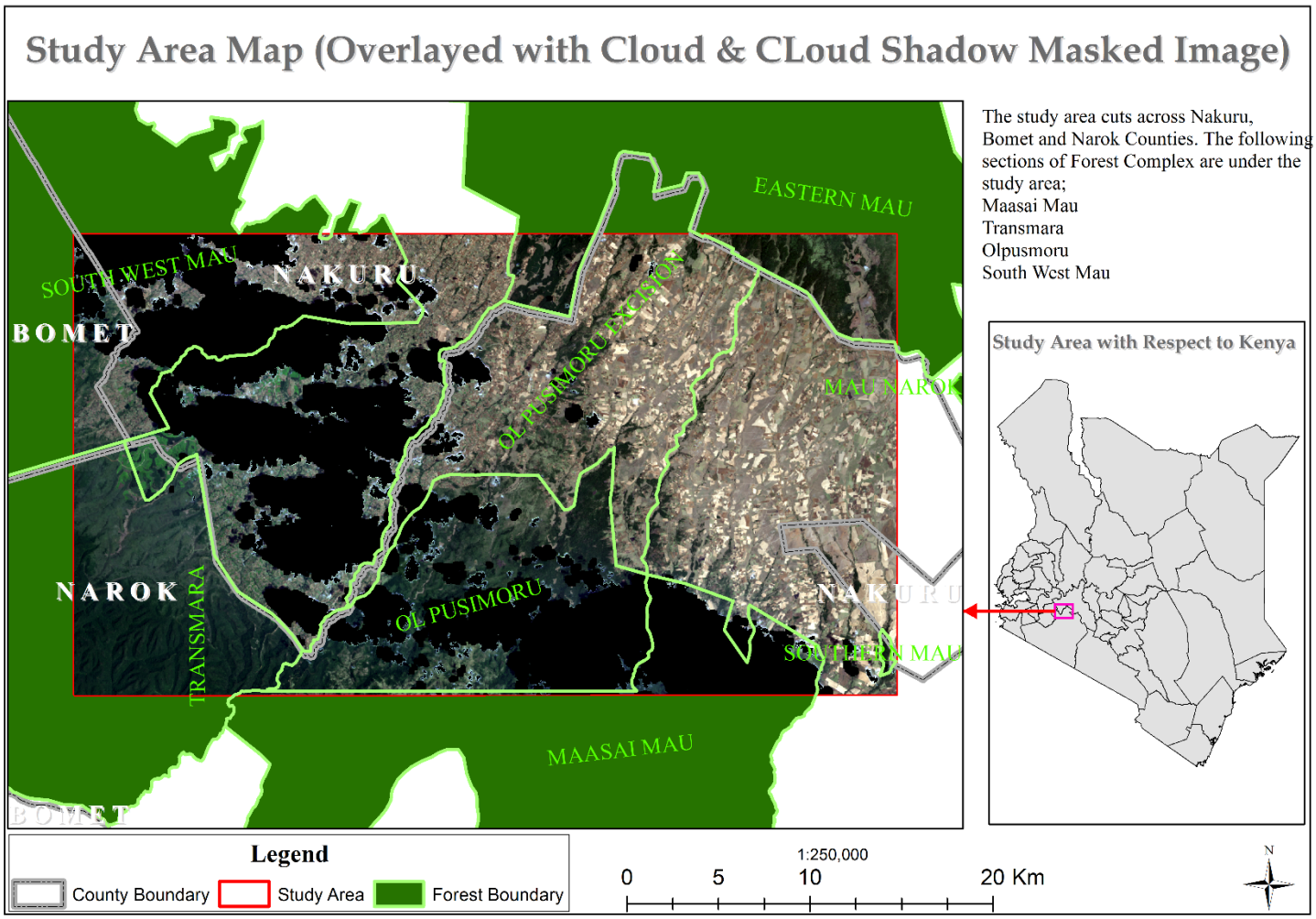

Plate 4.5: Cloud and Cloud Shadow Masked Image Linked with Study Area

4.2 Cloud and Cloud Shadow Free Image

The interpolation technique was used to get missing information for the cloud and cloud shadow masked pixels and the resulting image is as shown in *Plate 4.6* .Visual examination of the results shows that the areas masked as cloud and cloud shadow areas were well interpolated and the image information beneath them revealed. However, the interpolated areas still show the boundary outlines of the removed clouds and their shadows and there is contrast imbalance between the interpolated areas and other areas of the image. This is due to the fact that during interpolation, pixels with the closest value to the pixel being interpolated were used to replace the cloud and cloud shadow contaminated pixels and post cloud removal processing is required to address this problem.

Plate 4.6: Interpolated Cloud and Cloud Shadow Free Image

seen, however, contrast difference between the interpolated areas and the non-interpolated areas could visually be seen making the image not smooth. As a result of the contrast difference between the interpolated and non-interpolated areas, the cloud and cloud shadow boundaries could visually be seen after close observation. The thin clouds which were not detected were also visible in the interpolated image and they obscured details in their areas of presence. The cloud free image linked with the study area is as shown in *Plate 4.7*.

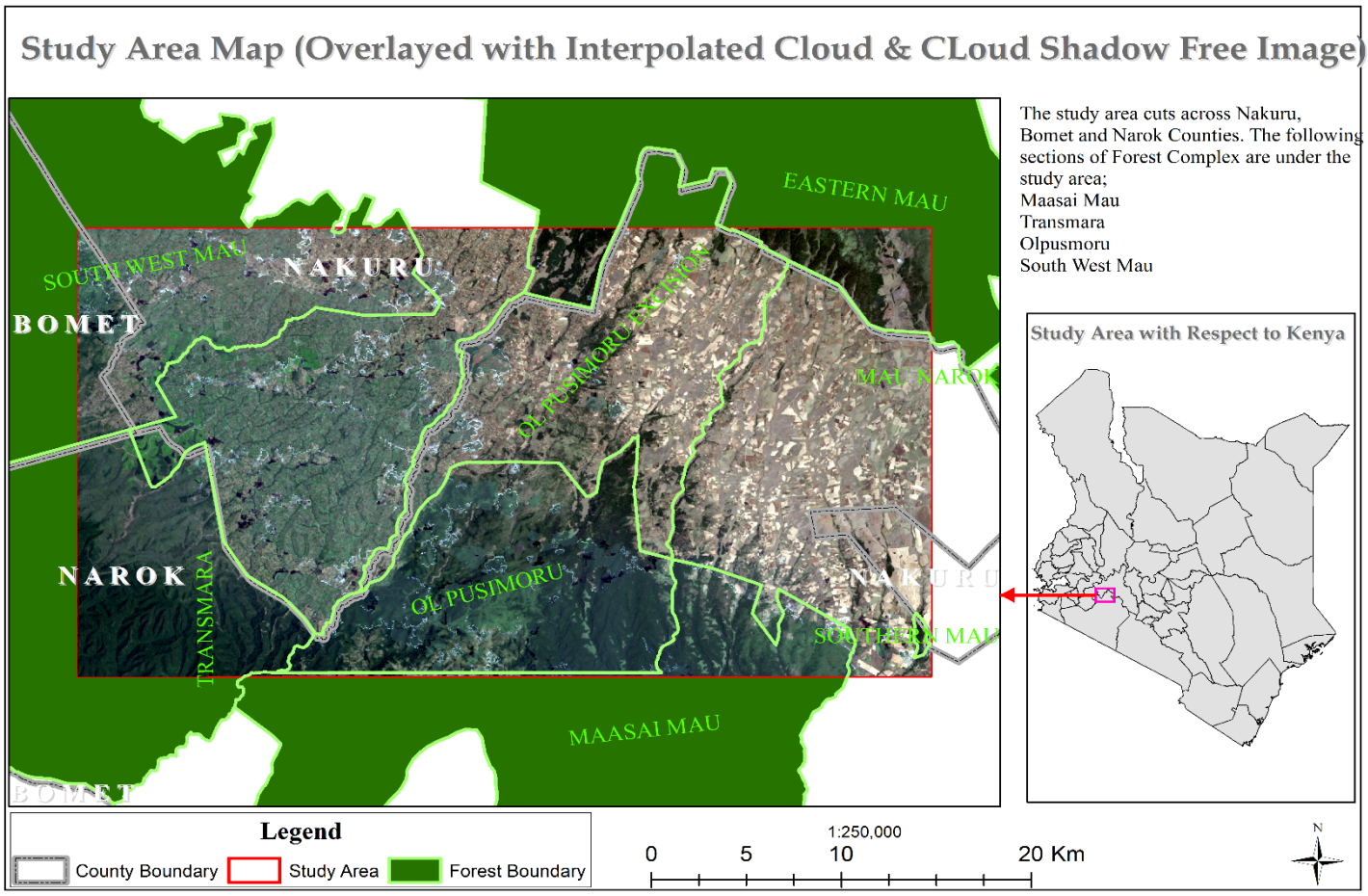

Plate 4.7: Interpolated Cloud Free Image Linked with Study Area

4.3 Cloud and Cloud Shadow Free Image Land Cover Analysis

The analysis of the results is as discussed in the following subsections. Focus was done on verification of correctness of information revealed below the cloud and cloud shadow interpolated areas as well as comparisons between land cover types between the cloud free image and the cloud image.

4.3.1 Verification of Results

Results verification was done using a high-resolution QuickBird cloud free image whose acquisition time was same month with that of the cloud contaminated optical image so as to verify whether land cover types revealed in the interpolated image are the same as the ones in the high-resolution cloud free image. This is as shown in *Plate 4.8* and *Plate 4.9*. Four samples of different locations of the cloud free interpolated image were taken and compared to their corresponding locations in the high-resolution image. The comparisons showed that the land cover features in the interpolated cloud free image were similar to their corresponding features in the high-resolution

image and this confirmed the correctness of the details revealed in the cloud image after interpolation.

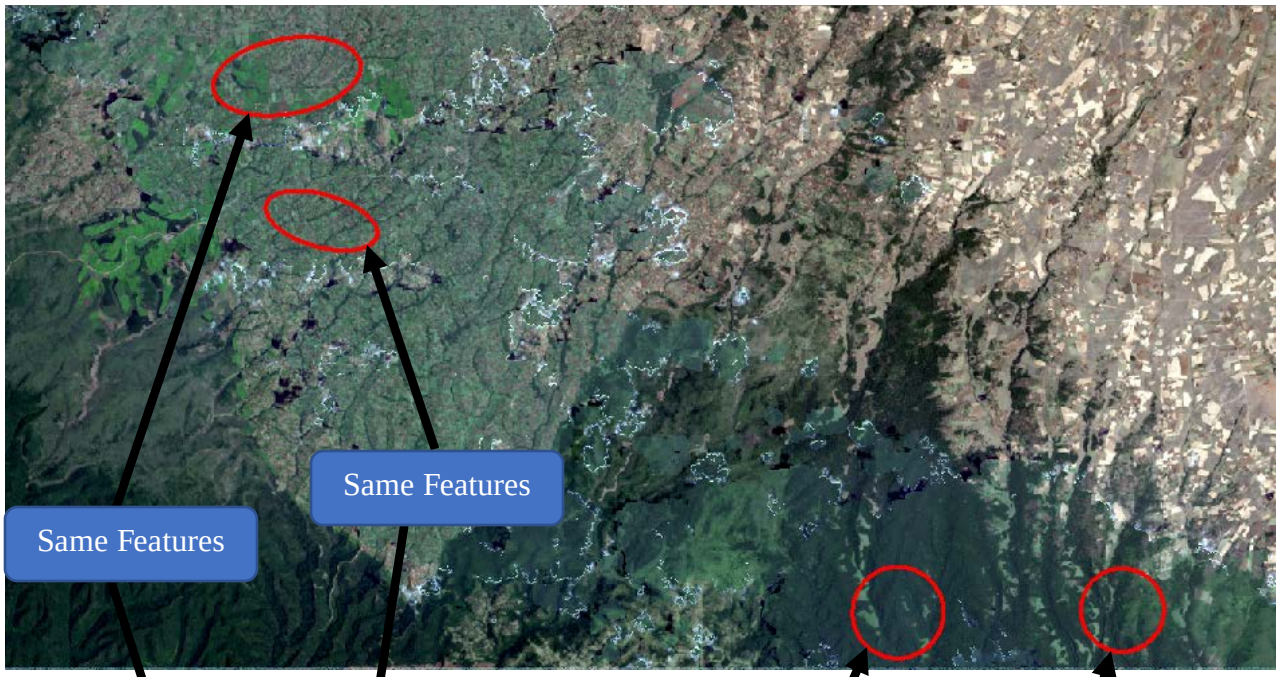

Plate 4.8: Interpolated Cloud Free Image

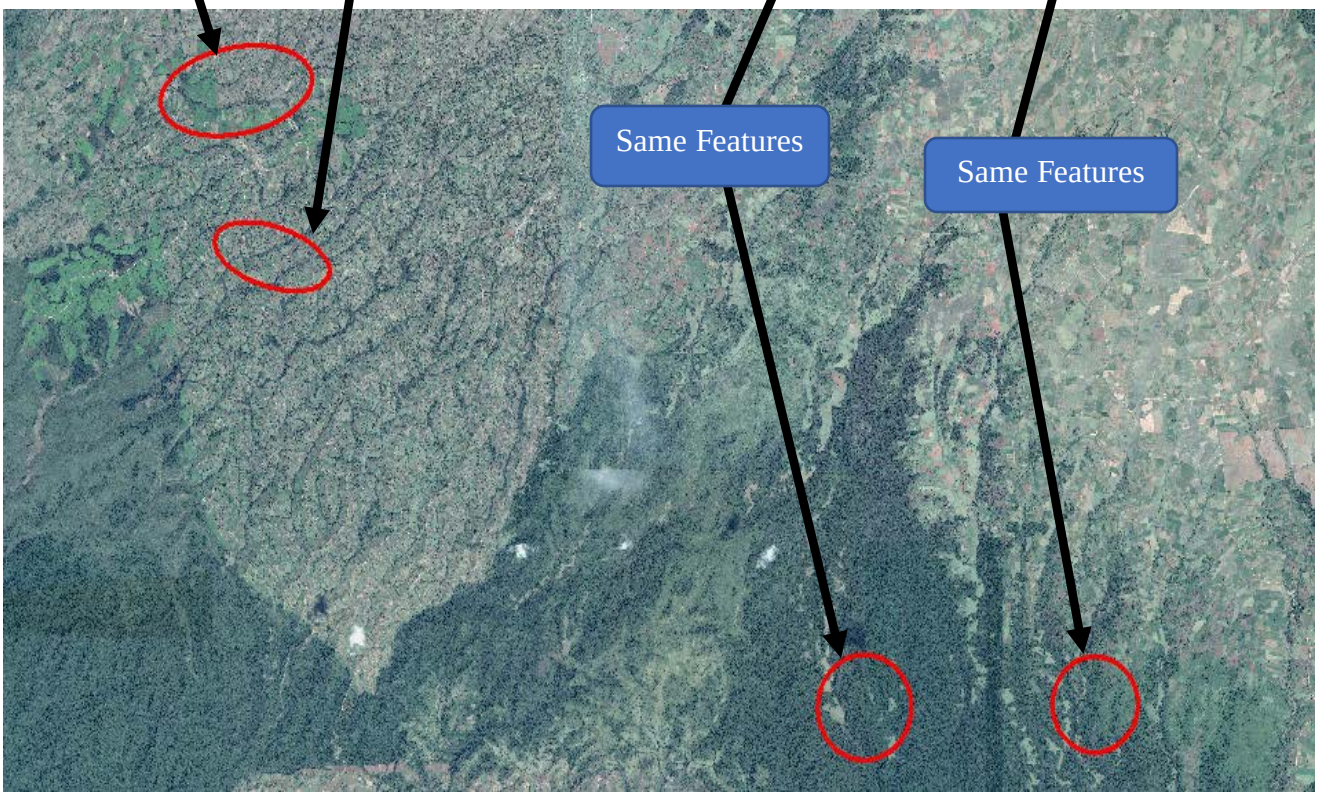

Plate 4.9: High Resolution Image

4.3.2 Test of Interpolated Image for Other Applications

In order to test the usability of the interpolated image for other applications like data capture through digitization, an attempt was made to digitize a linear feature cutting across interpolated and non-interpolated areas in the image. This was to test whether the features can be captured without any difficulties and rivers were digitized for this test and the results are as shown *Plate 4.10*

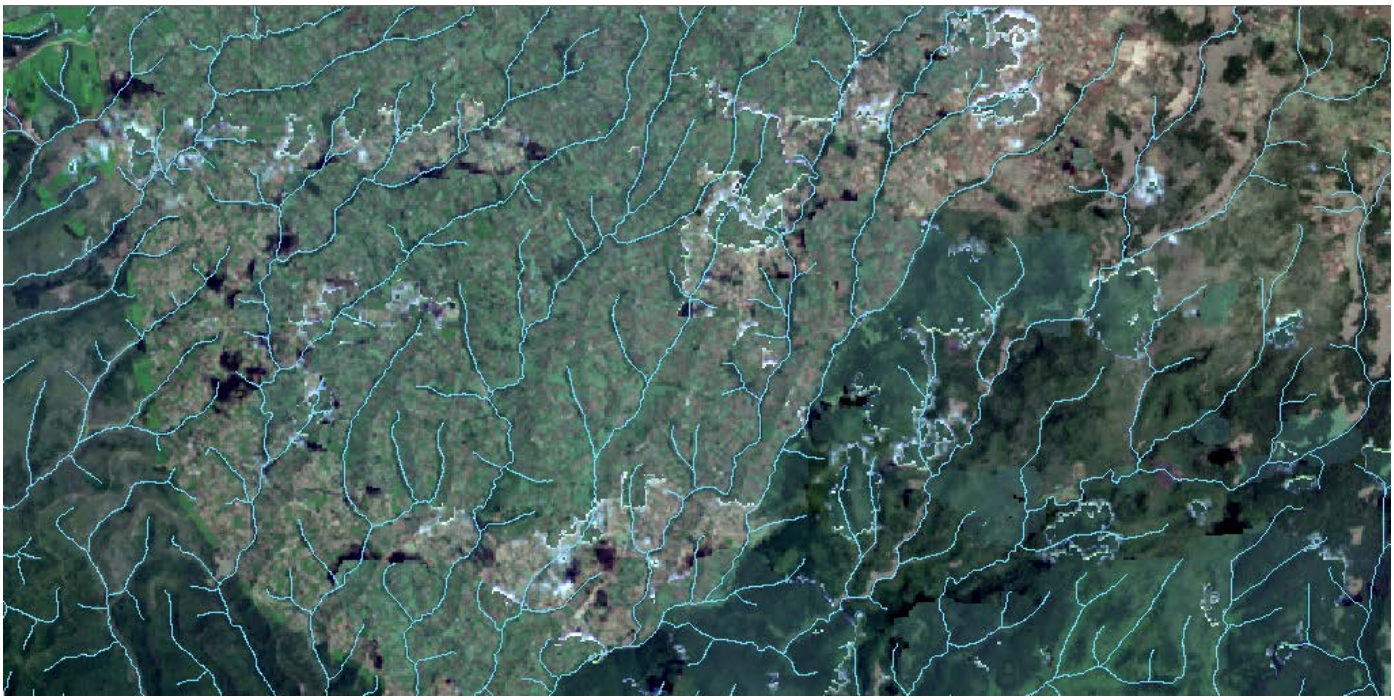

Plate 4.10: Test of Interpolated Image for Digitization

The usability of the interpolated image for other applications like data capture through digitization was done and it was found that data capture was done with ease except for the areas where thin clouds were not detected and masked.

4.3.3 Comparative Analysis for Land cover

This was done to demonstrate how the cloud free image can be used for Land Cover Mapping by comparing the cloud image and the interpolated cloud free image to show the land cover types revealed below the clouds after interpolation. *Plate 4.11* shows the farmland from the cloud image revealed in the interpolated image.

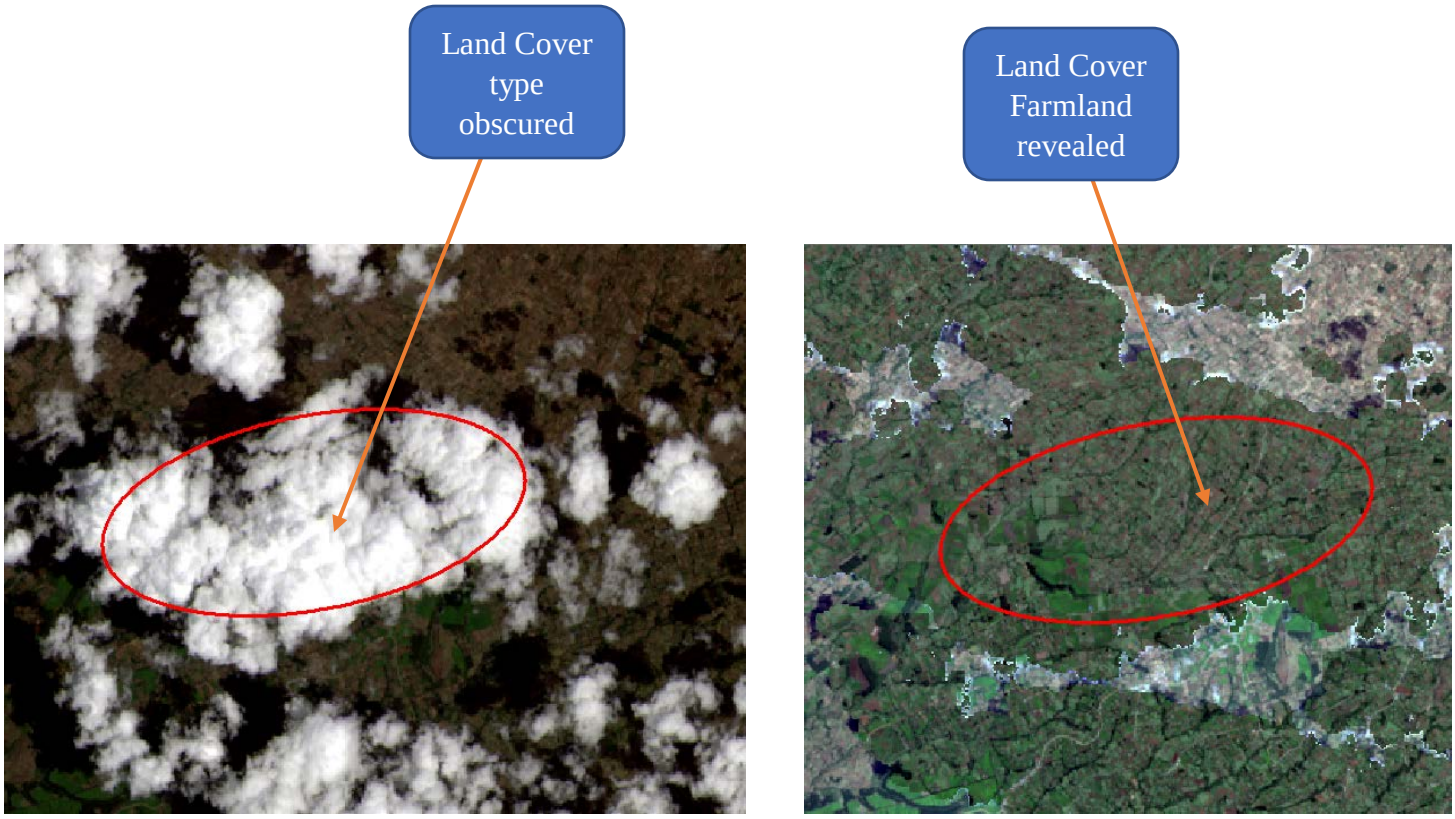

Plate 4.11: Cloud and Cloud Shadow Removal on Farmland Landcover

Another comparison between cloud contaminated image area and the interpolated cloud free image was done and the cloud free image revealed the cloud obscured details below the cloud cover in the cloud image. This is as shown in *Plate 4.12*

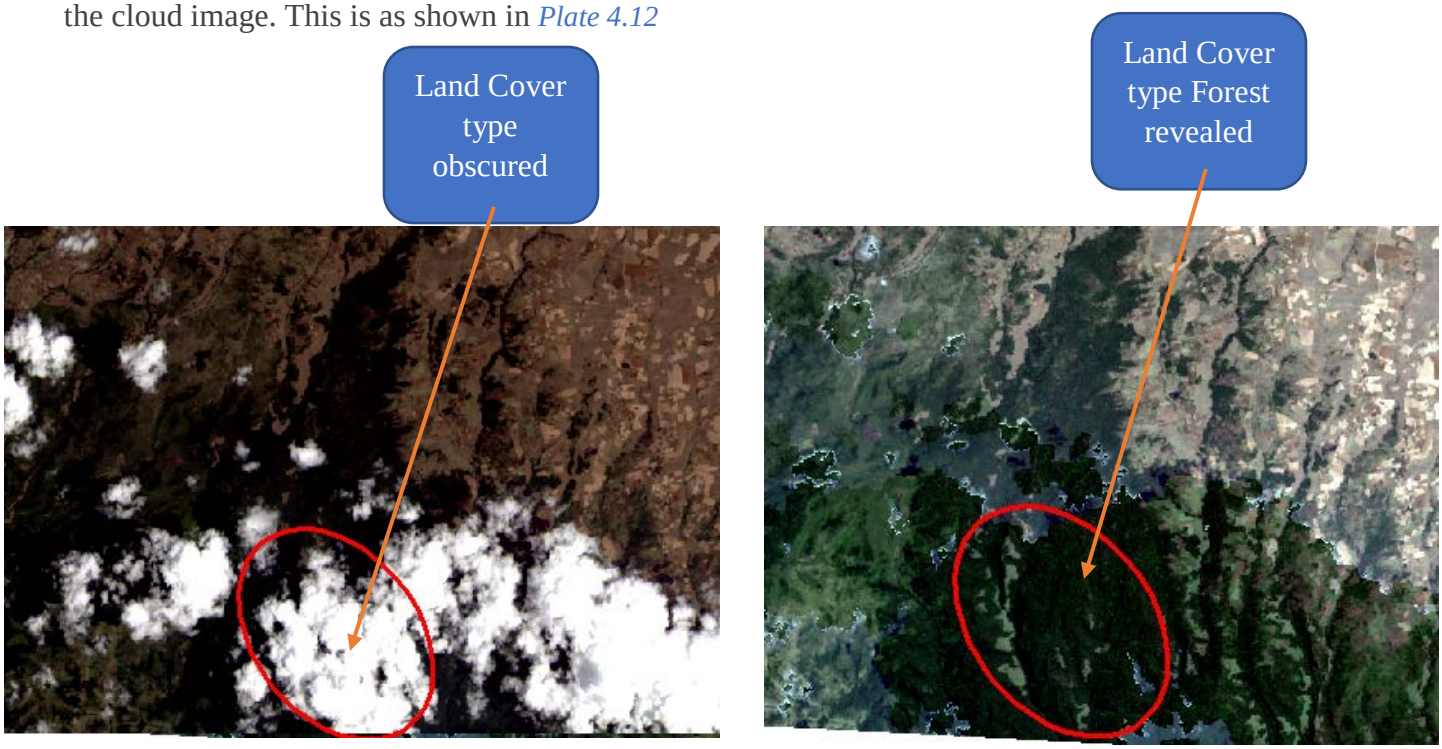

Plate 4.12:Cloud and Cloud Shadow Removal on Forest Landcover

4.4 Discussions of the Results

Thick clouds were defined using the TRRI (TRRI>60%), thin clouds were defined using CSI (-0.3<CSI<-0.2) while cloud shadows were defined by projecting the defined clouds with the average of distances and bearings measured from a sample of the defined clouds. Using the developed program function to define thick clouds using the defined thresholds of TRRI, thick clouds were successfully detected and masked out. Using the developed program function to detect thin clouds by using the defined threshold of CSI, majority of thin clouds were successfully detected and masked out but there were still some remnants of thin clouds which still remained undetected. Using the developed program for cloud shadow detection and by use of average of distances and bearings of clouds to their cloud shadows, cloud shadows were successfully detected and masked out although there were instances of over-detection and under-detection. To address the problem of under-detection, regional growth of the already detected cloud shadow areas was done so as to detect the un-detected cloud shadow areas which although it solves the problem, it increases the computational during interpolation. The cloud and cloud shadow masked image showed that all the detected cloud and cloud shadow contaminated pixels were well masked out leaving only the cloud and cloud shadow free pixels.

The developed program function for cloud and cloud shadow removal through interpolation was applied on the cloud and cloud shadow masked image and the resulting cloud free image looked good with all the image information obscured by cloud and cloud shadows revealed. However, the resulting cloud free image still had contrast mismatch and artifacts boundary between the interpolated and non-interpolated parts of the optical image hence making the cloud free interpolated image not smooth. Image verification was done so as to confirm the revealed image details in the cloud and cloud shadow areas of the interpolated optical image are the correct details by comparing it with another acquired high resolution cloud free satellite image of the same area acquired at the same time. The results of the verification confirmed that the details revealed in the cloud and cloud shadow obstructed areas were the correct image details because comparison between cloud and cloud shadow obstructed areas with their corresponding location in the acquired cloud free high-resolution image showed similar image features. The interpolated cloud and cloud shadow free image was also subjected to tests on usability of the image to other remote sensing applications like data capture through digitization and the results looked very good with the digitized features (rivers) being captured with ease because they were easily visible.

Chapter 5: Conclusions and Recommendations

5.1 Conclusions

Many approaches or techniques have been used towards cloud and cloud shadow removal but in this research, a technique has been presented which makes use of both optical and microwave data for cloud and cloud shadow removal using ALOS data. Development of a program function to define thick clouds was successfully achieved using MATLAB programming language where Total Reflectance Radiance Index (TRRI) was used to distinguish between thick and non-thick cloud pixels. Using the program, thick clouds contaminated pixels of the optical satellite image were detected and masked out successfully. Total Reflectance Radiance Index (TRRI) is therefore a very good index for detection of all thick clouds in an optical image and can be applied in all optical images because it is computed using the reflective bands in an optical image. Thin Clouds detection program function was also successfully developed using MATLAB programming language by making use of Cloud Soil Index (CSI) to define thin clouds. Although majority of the thin clouds were detected, there were still some patches which still remained undetected. Therefore, CSI does not detect all the thin clouds present in the optical image as some remnants could still be seen in the image despite the developed function successfully detecting and masking thin clouds pixels based on input thresholds.

Development of a program function to detect cloud shadows was successfully achieved using MATLAB programming language where cloud shadows were detected by projecting the average of distances and bearings measured from a sample of cloud patches to their corresponding shadows. However, it is important to note that this technique resulted in some cloud shadows going undetected and some non-cloud shadow areas being detected as cloud shadows. A program function for cloud and cloud shadow removal from optical image using interpolation technique was successfully achieved and using the program, a cloud free interpolated image was realized. The interpolation program function developed for cloud removal worked very well and all the masked areas details were revealed and therefore use of optical and microwave data for cloud and cloud shadow removal can be adopted henceforth as an addition to the existing approaches for cloud and cloud shadow removal. Testing of the cloud and cloud shadow free image through land cover analysis was done and it can be concluded that the actual land cover types obscured by the

clouds and their shadows were successfully revealed and verification was successfully done. Verification was done by comparing the land cover types in the cloud and cloud shadow obscured areas with their corresponding parts in the acquired cloud free high-resolution satellite image which also confirmed similar land cover types.

5.2 Recommendations

The developed cloud and cloud shadow removal algorithm worked very well and cloud and cloud shadows were successfully removed, however, the following recommendations are proposed;

i. Further research needs to be carried out for a more rigorous approach towards detection of thin clouds because using CSI, majority of the thin clouds were detected but there were still some which remained undetected.
ii. The technique used in detection of clouds shadows needs further research to improve its accuracy especially an approach which takes in to account the height of the clouds. This is because the used approach either had an over-detection or under-detection of cloud shadows.
iii. Lastly new satellite developers need to consider the possibility of incorporating both optical and microwave sensor onboard the same satellite so as to make data availability for this approach easily accessible and cheap.

References

Articles in journals

Arvidson, T., J. Gasch, and S.N. Goward. 2001. "Landsat 7's long term acquisition plan – An innovative approach to building a global archive." *Remote Sensing of Environment* 78: 13–26.

Aydınm, Abdurrahim, and Remzi Eker. 2017. "Forest mapping against rockfalls on a regional scale in Inebolu of Turkey." *Journal of the Faculty of Forestry Istanbul University* 67 (2): 136-149.

Braaten, Justin D., Warren B. Cohen, and Zhiqiang Yang. 2015. "Automated cloud and cloud shadow identification in Landsat MSS imagery for temperate ecosystems." *Remote Sensing of Environment* 169: 128-138.

Candra, D. S., S. Phinn, and P. Scarth. 2016. "Cloud And Cloud Shadow Masking Using Multi-Temporal Cloud Masking Algorithm In Tropical Environmental." *The International Archives of the Photogrammetry, Remote Sensing and Spatial Information Sciences* 1-6.

Chao-Hung, Lin, Tsai Po-Hung, Lai Kang-Hua, and Chen. Jyun-Yuan. 2010. "Cloud Removal from Multitemporal Satellite Images Using Information Cloning." *IEEE Transactions on Geoscience and Remote Sensing* XX (XX, XXX XXX): 1-10.

Chen, Bin, Bo Huang, Lifan Chen, and Bing Xu. 2017. "Spatially and Temporally Weighted Regression:A Novel Method to Produce Continuous Cloud-Free Landsat Imagery." *Ieee Transactions On Geoscience And Remote Sensing* 55 (1): 27 - 37.

Chen, J., X. Zhu, J. E. Vogelmann, F. Gao, and S. Jin. 2011. "A Simple and Effective Method for Filling Gaps in Landsat ETM+SLC-Off Images." *Remote Sensing of Environment* 115: 1053–64.

Fisher, Adrian. 2014. "Cloud and Cloud-Shadow Detection in SPOT5 HRG Imagery with Automated Morphological Feature Extraction." *Remote Sensing Open Access Journal* 6: 776-800.

Gao, B.C., A.F. Goetz, and W.J. Wiscombe. 1993. "Cirrus cloud detection from airborne imaging spectrometer data using the 1.38 μm water vapor band." *Geophysical Research Letters* 20 (4): 301–304.

Ghosh, Radha Rani, M. Shahjahan Ali, Ashrafunnahar Hena, and H. Rahman. 2012. "A Simple Cloud Detection Algorithm Using NOAA-AVHRR Satellite Data." *International Journal of Scientific & Engineering Research* 3 (6).

Goodwin, Nicholas R., Lisa J. Collett, Robert J. Denham, Neil Flood, and Daniel Tindall. 2013. "Cloud and cloud shadow screening across Queensland, Australia: An automated method for Landsat TM/ETM + time series." *Remote Sensing of Environment* 134: 50-65.

Hagolle, O., M. Huc, Pascual D. Villa, and G. Dedieu. 2010. "A multi-temporal method for cloud detection, applied to FORMOSAT-2, VENμS,LANDSAT and SENTINEL-2 images." *Remote Sensing of Environment* 114: 1747-1755.

Hégarat-Mascle, Sylvie Le, and Cyrille André. 2009. "Use of Markov Random Fields for automatic cloud/shadow detection on high resolution optical images." *ISPRS Journal of Photogrammetry and Remote Sensing* 64: 351-366.

Huang, Chengquan, Nancy Thomas, Samuel N. Goward, Jeffrey G. Masek, Zhiliang Zhu, John R. G. Townshend, and James E. Vogelmann. 2010. "Automated masking of cloud and cloud shadow for forest change analysis using Landsat images." *International Journal of Remote Sensing* 31 (20): 5449–5464.

Hughes, M. Joseph, and J. Daniel Hayes. 2014. "Automated Detection of Cloud and Cloud Shadow in Single-Date Landsat Imagery Using Neural Networks and Spatial Post-Processing." *Remote Sensing Open Access Journal* 6: 4907-4926.

Irish, Richard R, John L. Barker, Samuel N. Goward, and Terry Arvidson. 2006. "Characterization of the Landsat-7 ETM+Automated Cloud-Cover Assessment (ACCA) Algorithm." *Photogrammetric Engineering & Remote Sensing* 72 (10): 1179-1188.

Jin, Suming, Collin Homer, Limin Yang, George Xian, Joyce Fry, Danielson Patrick, and Philip A. Townsend. 2013. "Automated cloud and shadow detection and filling using two-date Landsat imagery in the USA." *International Journal of Remote Sensing* 34 (5): 1540-1560.

Kalkan, Kaan, and Derya Maktav. 2017. "Segmentation Based Cloud and Cloud Shadow Detection in Satellite Imagery." *Journal of Aeronautics and Space Technologies* 10 (1): 45-54.

Leckie, Donald G. 1990. "Advances in remote sensing technologies for forest survey and management." *Canadian Journal of Forest Research* 20 (4): 464-483 .

Loveland, T R, B. C. Reed, J. F. Brown, D. O. Ohlen, Z. Zhu, L. Yang, and J.W Merchant. 2010. "Development of a global land cover characteristics database and IGBP DISCover from 1 km AVHRR data." *International Journal of Remote Sensing* 21 (6&7): 1303–1330.

Luo, Y., A. Trishchenko, and K. Khlopenkov. 2008. "Developing clear-sky, cloud and cloud shadow mask for producing clear-sky composites at 250-meter spatial resolution for the seven MODIS land bands over Canada and North America." *Remote Sensing of Environment* 112 (12): 4167–4185.

Meng, Qingmin, Bruce E. B orders, Chris J. Cieszewski, and Marguerite Madden. 2009. "Closest Spectral Fit for Removing Clouds and Cloud Shadows." *Photogrammetric Engineering & Remote Sensing* 75 (9): 569–576.

Nguyen, T., and T. Ryutaro. 2009. "Cloud Removal of Optical Images using SAR data for ALOS Applications." *Journal of the Remote Sensing Society of Japan* 1-8.

Ramya, P., S. KarthiPrem, and A. Nithyasri. 2014. "Cloud Removal in High Satellite Images Using Discrete Wavelet Transform." *International Journal of Innovations & Advancement in Computer Science* 3 (2).

Roy, D.P., and J. Ju. 2008. "The availability of cloud-free Landsat ETM Plus data over the conterminous United States and globally." *Remote Sensing of Environmental* 1196-1211.

Sawaya, Kali E., Leif G. Olmanson, Nathan J. Heinert, Patrick L. Brezonik, and Marvin E. Bauer. 2003. "Extending satellite remote sensing to local scales: land and water resource monitoring using high-resolution imagery." *Remote Sensing of Environment* 88: 144– 156.

Shen, Yang, Yong Wang, Haitao Lv, and Hong Li. 2015. "Removal of Thin Clouds Using Cirrus and QA Bands of Landsat-8." *Photogrammetric Engineering & Remote Sensing* 81 (9): 721-731.

Stournara, Panagiota, Maria Tsakiri-Strati, and Petros Patias. 2013. "Detection and removal of cloud and cloud shadow contamination from hyperspectral images of Hyperion sensor." *South-Eastern European Journal of Earth Observation and Geomatics* 2 (1).

Wang, B., A Ono, K. Muramatsu, and N. Fujiwara. 1999. "Automated detection and removal of cloud and their shadow from Landsat TM images." *IEICE Transactions on Information and Systems* 1.

Yang, S., W. Yong, L. Haitao, and Q. Jiang. 2015. "Removal of Thin Clouds in Landsat-8 OLI Data with Independent Component Analysis." *Remote Sensing Open Access Journal* 1-20.

Yin, He, Asia Khamzina, Dirk Pflugmacher, and Christopher Martius. 2017. *Forest cover mapping in post-Soviet Central Asia using multi-resolution remote sensing imagery*. Bonn: University of Bonn.

Zhang, Y., W. B. Rossow, A. A. Lacis, V. Oinas, and M. I. Mishchenko. 2004. "Calculation of radiative fluxes from the surface to top of atmosphere based on ISCCP and other global data sets : Refinements of the radiative transfer model and the input data." *Journal of Geophysical Research* 109 (19): 191-205.

Zhu, Z., S. Wang, and C. E. Woodcock. 2015. "Improvement and expension of the Fmask algorithm: cloud, cloud shadow, and snow detection for Landat 4-7, 8, and Sentinel 2 images." *Remote Sensing and Environment* 159: 269-277.

Zhu, Zhe, and Curtis E. Woodcock. 2014. "Automated cloud cloud shadow and snow detection in multitemporal Landsat data." *Remote Sensing of Environment* 152: 217–234.

Zhu, Zhe, and Curtis E. Woodcock. 2011. "Object-based cloud and cloud shadow detection in Landsat imagery." *Remote Sensing of Environment* 118: 83–94.

Reports

Food and Agriculture Organization . 2015. *The Global Forest Resources Assessment.* Rome: FAO.

Food and Agriculture Organization. 2008. *FAO Land Cover Mapping Initiatives.* Rome: FAO.

Feng, C., and J. Ma. 2004. *An Improved Method for Cloud Removal in ASTER Data Change Detection.* Beijing: Chinese Academy of Sciences.

Gerlinger, Katrin. 2013. *Remote Sensing Application Potentials in Africa.* Berlin: Office of Technology Assessment at the German Bundestag.

GoK. 2017. *The Kenya Space Agency Order.* Nairobi: GoK Printer.

Goodwin, Robert F., and William D. Hudson. 2002. *Comparison of Air Photo and Satellite Image Sources for Updating Land Cover and Land Use Maps.* Michigan: Michigan State University.

Ministry of Environment and Mineral Resources, Kenya. 2012. *Kenya Wetlands Atlas.* Nairobi:

Office of the Prime Minister. 2009. *The Mau Forest Complex- Frequently Asked Questions.* Nairobi: KWS.

Wheeler, James. 2011. *Forest Monitoring of the Congo Basin using Synthetic Aperture Radar (SAR).* Leicester: University of University of Leicester.

Web-based articles

Japan Aerospace Exploration Agency. 2016. *Advanced Land Observing Satellite "DAICHI" (ALOS).* December 12. http://www.eorc.jaxa.jp/ALOS/en/about/avnir2.htm.

Regional Center for Mapping of Resources for Development. 2016. *http://www.rcmrd.org.* Accessed June 20, 2017. http://www.rcmrd.org/rcmrds-land-cover-mapping-group-to-support-the-system-for-land-based-emissions-estimation-in-kenya/.

Standard Media Group. 2015. *Kenya to launch space centre.* June 25. https://www.standardmedia.co.ke/article/2000167230/kenya-to-launch-space-centre.

Proceedings

Ibba, Roberto. 2007. "44th Session of Scientific and Technical Sub-Committee of COPUOS." *The San MArco Project in Malindi Kenya,The Italian Contribution to SPace Technology for Sustainable Development* . WIEN: Italian Space Agency. 1-19.

Irish, Richard R. 2000. "Landsat 7 Automatic Cloud Cover Assessment." *Proceedings of SPIE* Vol. 4049: 355-438.

Books

Aggarwal, Shefali. 2005. *Principles of Remote Sensing.* Dehra Dun: Indian Institute of Remote Sensing.

Canada Centre for Remote Sensing. 2016. *Fundamentals of Remote Sensing.* Ottawa: Canada

James, B. Campbell, and H. Wynne Randolph. 2011. *Introduction to Remote Sensing.* New York: The Guilford Press.

Klaus, Tempfli, Kerle Norman, and C. Huunerman Gerrit. 2009. *Principles of Remote Sensing.* Enschede: The International Institute for Geo-Information Science and Earth Observation.

Smithson, Peter, Ken Addison, and Ken Atkinson. 2008. *Fundamentals of the physical environment.* 4th edition. Routledge, NewYork.

Appendix A

Appendix A1: The developed MATLAB Algorithm

```
%% Reading Image Bands in to Array From and the Projection Information

[Band1,R]=geotiffread('F:\Thesis\Images\0000146611_001001_ALAV2A191273610\01-ALAV2A191273610-O1B2R_U.tif');

[Band2,R]=geotiffread('F:\Thesis\Images\0000146611_001001_ALAV2A191273610\02-ALAV2A191273610-O1B2R_U.tif');

[Band3,R]=geotiffread('F:\Thesis\Images\0000146611_001001_ALAV2A191273610\03-ALAV2A191273610-O1B2R_U.tif');

[Band4,R]=geotiffread('F:\Thesis\Images\0000146611_001001_ALAV2A191273610\04-ALAV2A191273610-O1B2R_U.tif');

%% Setting the Gain and Offset Co-efficients for Computing each Band Radiance

Gain_B1=0.5880;

Gain_B2=0.5730;

Gain_B3=0.5020;

Gain_B4=0.5570;

Offset_B1=0.0000;

Offset_B2=0.0000;

Offset_B3=0.0000;

Offset_B4=0.0000;

%% Computing each Band Radiance: L? = DN*Gain + Offset

Band1_Rad= double(Band1)*double(Gain_B1)+double(Offset_B1);

Band2_Rad= double(Band2)*double(Gain_B2)+double(Offset_B2);

Band3_Rad= double(Band3)*double(Gain_B3)+double(Offset_B3);

Band4_Rad= double(Band4)*double(Gain_B4)+double(Offset_B4);

%% Setting Parameters for Computing Reflectance; ? = ?*L?*d2 /(ESUN?)*Sin?

d=1.0103742;

ESUN_B1=1943.3;

ESUN_B2=1813.7;

ESUN_B3=1562.3;

ESUN_B4=1076.5;

theta=65.20;
```

```
%% Computing Reflectance; ? = *L?*d2 /(ESUN?)*Sin?
Band1_Ref=double(Band1_Rad)*double(pi)*double(d^2)/(double(ESUN_B1)*sind(theta));
Band2_Ref=double(Band2_Rad)*double(pi)*double(d^2)/(double(ESUN_B2)*sind(theta));
Band3_Ref=double(Band3_Rad)*double(pi)*double(d^2)/(double(ESUN_B3)*sind(theta));
Band4_Ref=double(Band4_Rad)*double(pi)*double(d^2)/(double(ESUN_B4)*sind(theta));
%% Computing Total Reflectance Radiance Index  (TRRI); TRRI= (b2+ 2*(b3+b4+b5+b6)+b7)/2 for Landsat
% where b2, b3 ... b7 is TOA or surface reflectance
% ALOS AVNIR-2 Images; TRRI= (b1+2*(b2+b3)+b4)/2
TRRI= ((Band1_Ref+2*(Band2_Ref+Band3_Ref)+Band4_Ref)/2)*100;
%% Writing the Final TRRI Image
coordRefSysCode = 32736;
filename = 'TRRI.tif';
geotiffwrite(filename, TRRI, R,'CoordRefSysCode',coordRefSysCode);
%% Computing the Cloud Soil Index (CSI)Band1-Band4/Band1+Band4 and writing it as an Image
CSI= double(Band1_Ref-Band4_Ref)./(Band1_Ref+Band4_Ref);
filename1 = 'CSI.tif';
geotiffwrite(filename1, CSI, R,'CoordRefSysCode',coordRefSysCode);
%% Defining Cloud Using the TRRI Index; Any Pixel greater than 60 is a cloud Pixel
idx1=find(TRRI>=60);
idx2=find(CSI>=-0.3 and CSI<=-0.2);
Band1_Cloud=Band1;
Band2_Cloud=Band2;
Band3_Cloud=Band3;
Band4_Cloud=Band4;
%%  Writing the TRRI Image Combining the 3 Bands
filename2='TRRI.tif';
geotiffwrite(filename2, TRRI, R,'CoordRefSysCode',coordRefSysCode);
%% All Cloud Pixels are being allocated Value 0 in all Bands
Band1_Cloud(idx1)=0;
Band2_Cloud(idx1)=0;
Band3_Cloud(idx1)=0;
Band4_Cloud(idx1)=0;
```

```
%%Combining the Bands and writing the cloud masked image
Cloud_Masked_Image=cat(3,Band1_Cloud,Band2_Cloud,Band3_Cloud);
filename3='Cloud_Masked_Image.tif';
geotiffwrite(filename3, Cloud_Masked_Image, R,'CoordRefSysCode',coordRefSysCode);
%% Masking thin Cloud Pixels by allocating value zero and writing the image
Band1_Cloud(idx2)=0;
Band2_Cloud(idx2)=0;
Band3_Cloud(idx2)=0;
Band4_Cloud(idx2)=0;
Cloud_thin_Masked=cat(3,Band1_Cloud,Band2_Cloud,Band3_Cloud);
filename4='Cloud_thin_Masked.tif';
geotiffwrite(filename4,Cloud_thin_Masked, R,'CoordRefSysCode',coordRefSysCode);
%% Masking cloud shadows by projectingcloud pixels using distance and Bearing
Distance=837.931;
Bearing=240.1550378;
idx4 = knnsearch(Band1_Cloud(idx1),Distance,Bearing);
Band1_Cloud(idx4)=0;
Band2_Cloud(idx4)=0;
Band3_Cloud(idx4)=0;
Band4_Cloud(idx4)=0;
%% Writing the cloud shadow Masked Image
Cloud_Sgadow_Masked=cat(3,Band1_Cloud,Band2_Cloud,Band3_Cloud);
filename5='Cloud_Shadow_Masked.tif';
geotiffwrite(filename5,Cloud_Shadow_Masked, R,'CoordRefSysCode',coordRefSysCode);
%% Interpolation between cloud Image and Radar Image
All_Bands_Masked_Image=cat(Band1_Cloud,Band2_Cloud,Band3_Cloud);
idx5=find(All_Bands_Masked_Image==0);
SAR=geotiffread('F:\Thesis\Images\Thesis_Works\SAR.tif');
Cloud_Pixels=SAR(idx5);
SAR_Norm=SAR;
SAR_Norm(idx5)=0;
%% Interpolating the SAR Image
```

```
SAR_Norm_CV=reshape(SAR_Norm,[],1);
idx6 = knnsearch(SAR_Norm_CV,Cloud_Pixels);
for i=1:idx5;
    if(Band1_Cloud(idx5)~=0);
    Band1_Cloud(idx5)=Band1_Cloud(idx6);
    Band2_Cloud(idx5)=Band2_Cloud(idx6);
    Band3_Cloud(idx5)=Band3_Cloud(idx6);
    end
end

%%Combining the interpolated Bands in to single image
Cloud_Free_Image=cat(Band1_Cloud,Band2_Cloud,Band3_Cloud);
filename6='Cloud_Free_Image.tif';
geotiffwrite(filename6,Cloud_Free_Image, R,'CoordRefSysCode',coordRefSysCode);
```